Title: mRNA structure determines specificity of a polyQ-driven phase separation

Authors: Erin M. Langdon[1], Yupeng Qiu[4], Amirhossein Ghanbari Niaki[4], Grace A. McLaughlin[1], Chase Weidmann[2], Therese M. Gerbich[1], Jean A. Smith[1], John M. Crutchley[1], Christina M. Termini[5], Kevin M. Weeks[2], Sua Myong[4], and Amy S. Gladfelter[1,3]*

Affiliations:

[1]Department of Biology

[2]Department of Chemistry

 University of North Carolina at Chapel Hill

 Chapel Hill, NC 27599

[3]Marine Biological Laboratory

Woods Hole, MA 02543

[4]Department of Biophysics

 Johns Hopkins University

 Baltimore, MD 21218

[5]Division of Hematology/Oncology, Department of Medicine

University of California, Los Angeles

Los Angeles, CA 90095

*Correspondence to: amyglad@unc.edu

Abstract:

RNA promotes liquid-liquid phase separation (LLPS) to build membrane-less compartments in cells. How distinct molecular compositions are established and maintained in these liquid compartments is unknown. Here we report that secondary structure allows mRNAs to self-associate and determines if an mRNA is recruited to or excluded from liquid compartments. The polyQ-protein Whi3 induces conformational changes in RNA structure and generates distinct molecular fluctuations depending on the RNA sequence. These data support a model in which structure-based, RNA-RNA interactions promote assembly of distinct droplets and protein-driven, conformational dynamics of the RNA maintain this identity. Thus, the shape of RNA can promote the formation and coexistence of the diverse array of RNA-rich liquid compartments found in a single cell.

One Sentence Summary:

Identity in cellular, phase-separated compartments arises from RNA-RNA complexes encoded by mRNA secondary structures.

Main Text:

Formation of non-membrane bound organelles through the condensation of macromolecules is a recently appreciated mechanism of intracellular organization. These liquid-like condensates form through liquid-liquid phase separation (LLPS) and are found in the cytoplasm and nucleus (*1*, *2*). A fundamental unsolved problem is how liquid droplets recruit distinct constituents and retain independent identities. RNA can drive LLPS and modulates the material properties of droplets (*3-6*), but it is unknown if RNA controls the identity and maintenance of coexisting liquid

compartments. Here we show mRNA secondary structure is required for droplet identity through directing interactions between mRNAs and RNA-binding proteins.

Whi3, a polyQ-containing, RNA-binding protein first identified in *Saccharomyces cerevisiae* (*7*), functions in morphogenesis, memory of mating, and stress responses, where it forms aggregates and associates with RNA-processing bodies (*8-11*). The homolog in the filamentous fungus *Ashbya gossypii* has one RNA recognition motif (RRM) and an expanded polyQ tract (Fig. S1A), and both regions promote self-assembly. In vitro, Whi3 polyQ-dependent LLPS is driven by specific RNAs encoding regulators of either the cell cycle (e.g. the cyclin *CLN3*) or actin (e.g. the formin *BNI1* and *SPA2*) (*3*). Distinct types of Whi3 droplets form in *Ashbya* cells: perinuclear *CLN3* droplets and *BNI1* droplets at sites of polarized growth at cell tips ((*12*, *13*), Fig. 1A and movie S1). These two types of droplets have different Whi3 levels and Whi3 incorporation rates (Fig. 1, B and C), suggesting they are structurally distinct.

The distinct droplet properties may depend on extrinsic features of the local cytosolic microenvironment or arise due to different droplet constituents. *CLN3* and *BNI1* mRNAs minimally co-localize in the cytoplasm by single molecule (sm) RNA F.I.S.H., although they were occasionally co-expressed by the same nucleus (Fig. 1, D and F). The lack of co-localization suggests there are intrinsic, compositional differences between droplets. In contrast, mRNA of the polarity regulator *SPA2*, frequently co-localized with *BNI1* mRNAs, especially at growth sites (Fig. 1, E and F). Thus, mRNAs encoding functionally related proteins co-localize, while functionally unrelated mRNAs do not. How can distinct Whi3-binding mRNAs segregate to different droplets in a common cytoplasm?

To address this question, we employed a reconstitution system to test if mRNA sequence was sufficient to generate droplet individuality (Fig. 2A). In vitro, as in cells, droplets composed of *BNI1* mRNA displayed higher Whi3 to RNA molar ratios than droplets made with *CLN3* mRNA (Fig. S1B). Remarkably, when *CLN3* mRNA was added to Whi3 droplets made with *BNI1* mRNA, *CLN3* preferentially assembled into new droplets, rather than incorporating into *BNI1* droplets (Fig. 2, B and C, S1C). In contrast, *BNI1* mRNA readily incorporated into preformed droplets (Fig. 2, B and C). Notably, *SPA2* mRNA incorporated into *BNI1* droplets (Fig. 2, B and C), and *CLN3* did not incorporate into *SPA2* droplets (Fig. S1D). Thus, as in cells, cyclin and polarity mRNAs assemble into distinct and immiscible droplets in vitro, indicating droplet identity is encoded by the mRNA.

mRNA sequences could influence droplet identity by favoring homotypic or specific heterotypic interactions between RNA molecules. To test for specific RNA-RNA interactions, we used a protein-free system to induce electrostatic-mediated phase transitions of the mRNA (*14*), where all mRNAs were capable of homotypic assembly into liquid or gel-like droplets (Fig. 2D). Strikingly, *CLN3* mRNAs had minimal co-localization with *BNI1* or *SPA2* mRNAs, whereas *BNI1* and *SPA2* were significantly more co-localized (Fig. 2 E–G). Thus, sequence-encoded features of the mRNA can underpin the assembly of distinct, immiscible structures.

We next investigated which features of the mRNA sequence generate specificity. An mRNA with scrambled *CLN3* coding sequence (*cln3 scr*) with intact Whi3-binding sites formed Whi3 droplets (Fig. S1E), but no longer showed specificity (Fig. 3, A and C). As the length, nucleotide

composition, and Whi3 binding sites were identical, we hypothesized the secondary structure could promote specificity. *CLN3* mRNA heated to 95ºC to disrupt secondary structure also readily incorporated into Whi3-*BNI1* droplets (Fig. 3, A and C). Melted *CLN3* mRNA that was slowly refolded (*CLN3* refold) showed significantly less recruitment than melted, but more than native *CLN3* (Fig. 3A and C). Mixing between melted *CLN3* and melted *BNI1* occurred in the presence of Whi3 and in RNA-only reactions, suggesting mixing is initiated by RNA-RNA interactions (Fig. S2). Thus, specificity information in *CLN3* mRNA can be eliminated by disrupting secondary structure.

To identify what features of *CLN3* mRNA secondary structure promote specificity, we performed SHAPE-MaP, which identifies highly flexible regions in RNA (*15*), to determine secondary structure changes, on native, refolded, and scrambled *CLN3* mRNA (Fig. 3D, S3A and B). The first 400 nucleotides in the *CLN3* sequence exhibited especially low SHAPE reactivity (Fig. S3C, purple shaded regions), suggesting many paired nucleotides and a highly folded structure. Refolded *CLN3* had a significant increase in SHAPE reactivity compared to native *CLN3* (Fig. S3A, p <0.001, Wilcoxon rank sum test), indicating a transition to a more unstructured state (Fig 3D and E). Melting and refolding thus allows the RNA to sample different conformations from those formed during transcription. As expected, *cln3 scr* showed a different SHAPE profile with dramatically altered secondary structure (Fig. 3 D and E, S3B).

We hypothesized secondary structure influences mRNA sorting, as stem-loops may selectively display or mask sequences capable of hybridizing with other RNAs. *CLN3* contains five complementary regions to *BNI1* (Fig. S4A), most of which had low SHAPE reactivity and

therefore were more structured (Fig. S4B), suggesting these regions are inaccessible for hybridizing with *BNI1*. We hypothesize these regions became available to pair with *BNI1* when *CLN3* is melted, causing the structure-dependent loss of droplet specificity. To test this hypothesis, oligonucleotides (*i.e.*, oligos) complementary to these regions were added to melted *CLN3* and significantly decreased the co-assembly with *BNI1*, restoring the formation of distinct *CLN3* droplets (Fig 3B and C). Additionally, *cln3sm*, a mutant perturbing structure and exposing complementarity, co-localized with *BNI1* transcripts in vitro and at polarity sites in cells (Fig. 3F, S5, >60% tips co-localized). Thus, secondary structure can regulate RNA sorting into distinct droplets through altering the capacity to form intermolecular interactions.

We next asked if exposed complementarity explains co-assembly of *BNI1* and *SPA2* into the same droplets. Indeed, SHAPE-MaP analysis of *BNI1* and *SPA2* showed complementary regions between these co-localizing mRNAs having significantly higher SHAPE reactivity and less structure compared to the *CLN3*/*BNI1* regions (Fig S4 and S6; $p < 0.002$, t test). Addition of complementary oligos to these regions disrupted co-localization in the presence of Whi3 and in RNA-only reactions (Fig. S7 A and B). We predicted that *CLN3* may self-assemble and indeed *cln3 codon*, a *CLN3* mutant whose codons have been randomized but Whi3 binding sites remain intact, does not co-localize with endogenous *CLN3* mRNA in cells, further supporting RNA-RNA interactions in co-assembly of related RNAs (Fig S7C). These data suggest RNA-RNA interactions based on intermolecular hybridization direct RNAs into the same or different droplets.

Does Whi3 protein influence the identity of droplets? The majority of Whi3 binding sites are exposed on stem loops in *CLN3*, *BNI1*, and *SPA2* (Fig. 3E, S8 and S9). Notably, refolding or scrambling the *CLN3* sequence rearranges the presentation of Whi3 binding sites (Fig. 3E). Therefore, RNA secondary structure may influence Whi3 binding and contribute to droplet composition and immiscibility in addition to RNA complexing. SHAPE-MaP of *CLN3* mRNA in the presence of Whi3 support that Whi3 binding sites are occupied by protein (Fig. 4A, S10A) and revealed that protein binding causes structural rearrangements (Fig. 4B). We therefore hypothesize Whi3 binding may have important contributions to structural rearrangements of target RNAs relevant to droplet identity.

To examine the consequence of Whi3 binding to RNA, we used smFRET (Fig. 4C) to measure the conformational dynamics of *CLN3* and *BNI1* mRNAs with and without Whi3 (*16*). In the absence of protein, *CLN3* RNA showed high FRET values indicative of a compacted state, while *BNI1* RNA showed lower FRET values, indicating a less compact state (Fig. 4D, purple shaded regions). Upon addition of Whi3, *CLN3* FRET values decreased, indicating more extended RNA conformations were induced, dependent on the ability of Whi3 to bind mRNA (Fig S10 B and C). In contrast, bound to Whi3, *BNI1* RNA showed a more substantial broadening of FRET values (Fig. 4D), indicating Whi3-*BNI1* complexes are more dynamic. Dwell-time analysis revealed Whi3-induced dynamics are three times faster for *BNI1* than *CLN3* (Fig. 4E). Different mRNAs thus react differentially in their intramolecular fluctuations to the presence of Whi3, providing an additional mode of RNA droplet regulation.

These FRET studies suggest Whi3 binding alters the conformational dynamics of target RNAs. We speculate these differential dynamics help maintain droplet identities established by RNA-RNA interactions. Once RNA-RNA interactions are formed, Whi3 binding may reduce the ability of the RNA to resample many alternate RNA structures to maintain the identity. Additionally, the slower fluctuations of *CLN3* bound to Whi3 may be one source of exclusion from the more rapidly fluctuating *BNI1*-Whi3 complexes in those droplets. Such dynamics may drive the droplet material properties reported previously (*3*) and serve as barriers to homogenization.

We show mRNA structure defines the ability of an RNA to engage in homo- or heteromeric interactions and thus drives specificity in the composition of liquid droplet compartments. This mechanism is likely relevant for the sorting of specific RNAs to other RNA-granules such as stress and P granules, and P-bodies (*17*, *18*). Future work will address the timing and location of how mRNA secondary structure influences selective uptake of cellular constituents into droplets. Protein binding to different RNAs can lead to varied dynamics of complexes, further distinguishing the physical properties of different droplets and promoting immiscibility of coexisting droplets (Fig. 4F). Given the large number of distinct, RNA-based condensates in the cell, these mechanisms are likely broadly relevant to explain how droplets achieve and maintain individuality.

References and Notes:

1. S. F. Banani, H. O. Lee, A. A. Hyman, M. K. Rosen, Biomolecular condensates: organizers of cellular biochemistry. *Nat Rev Mol Cell Biol*. **18**, 285–298 (2017).

2. Y. Shin, C. P. Brangwynne, Liquid phase condensation in cell physiology and disease. *Science*. **357**, eaaf4382–13 (2017).

3. H. Zhang *et al*., RNA Controls PolyQ Protein Phase Transitions. *Molecular Cell*. **60**, 220–230 (2015).

4. X. Zhang *et al*., RNA stores tau reversibly in complex coacervates. *PLoS Biol*. **15**, e2002183–28 (2017).

5. S. Elbaum-Garfinkle *et al*., The disordered P granule protein LAF-1 drives phase separation into droplets with tunable viscosity and dynamics. *Proc Natl Acad Sci USA*. **112**, 7189–7194 (2015).

6. Y. Lin, D. S. W. Protter, M. K. Rosen, R. Parker, Formation and Maturation of Phase-Separated Liquid Droplets by RNA-Binding Proteins. *Molecular Cell*. **60**, 208–219 (2015).

7. R. S. Nash, T. Volpe, B. Futcher, Isolation and Characterization of WHI3, a Size-Control Gene of Saccharomyces cerevisiae. *Genetics*, 1–12 (2001).

8. N. Colomina, F. Ferrezuelo, E. Vergés, M. Aldea, E. Garí, Whi3 regulates morphogenesis in budding yeast by enhancing Cdk functions in apical growth. *Cell Cycle*. **8**, 1912–1920 (2014).

9. F. Caudron, Y. Barral, A Super-Assembly of Whi3 Encodes Memory of Deceptive Encounters by Single Cells during Yeast Courtship. *Cell*. **155**, 1244–1257 (2013).

10. G. Schlissel, M. K. Krzyzanowski, F. Caudron, Y. Barral, J. Rine, Aggregation of the Whi3 protein, not loss of heterochromatin, causes sterility in old yeast cells. *Science*, 1–5 (2017).

11. K. J. Holmes, D. M. Klass, E. L. Guiney, M. S. Cyert, Whi3, an S. cerevisiae RNA-Binding Protein, Is a Component of Stress Granules That Regulates Levels of Its Target mRNAs. *PLoS ONE*. **8**, e84060–14 (2013).

12. C. Lee *et al*., Protein Aggregation Behavior Regulates Cyclin Transcript Localization and Cell-Cycle Control. *DEVCEL*. **25**, 572–584 (2013).

13. C. Lee, P. Occhipinti, A. S. Gladfelter, PolyQ-dependent RNA–protein assemblies control symmetry breaking. *J Cell Biol*. **208**, 533–544 (2015).

14. A. Jain, R. D. Vale, RNA phase transitions in repeat expansion disorders. *Nature*. **546**, 243–247 (2017).

15. M. J. Smola, G. M. Rice, S. Busan, N. A. Siegfried, K. M. Weeks, Selective 2′-hydroxyl acylation analyzed by primer extension and mutational profiling (SHAPE-MaP) for direct, versatile and accurate RNA structure analysis. *Nat Protoc*. **10**, 1643–1669 (2015).

16. Y. Kim, S. Myong, RNA Remodeling Activity of DEAD Box Proteins Tuned by Protein Concentration, RNA Length, and ATP. *Molecular Cell*. **63**, 865–876 (2016).

17. T. Trcek *et al*., Drosophila germ granules are structured and contain homotypic mRNA clusters. *Nature Communications*. **6**, 7962 (2015).

18. B. Van Treek *et al*., RNA self-assembly contributes to stress granule formation and defining the stress granule transcriptome. *Proc Natl Acad Sci USA*, 1–6 (2018).

Figure 1 Langdon et al.

A

115 →→→→→ 140

Time (min)

B

Mean Intensity (a.u)

2000

1000

200

Nuclei   Tips

C

Nuclei   Tips

Mean Intensity (a.u)

460
440

100

20

0   10   20

Time (min)

D

BNI1

CLN3

Merge

BNI1   *CLN3*   Nuclei

Nuclei

Tips

E

BNI1

SPA2

Merge

BNI1   *SPA2*   Nuclei

Nuclei

Tips

F

mRNA Fraction Colocalized

BNI1 & CLN3
BNI1 & SPA2

0.6

0.4

0.2

0.0

**   ***

Nuclei   Tips

Figure 1. Cyclin and Polarity complexes are spatially and physically distinct within the cell.

A. Top, Whi3 forms liquid droplets in *Ashbya gossypii*. Below, Whi3 droplets accumulate and fuse around nuclei. Green arrows denote polarity droplets. Pink arrows denote perinuclear droplets. Scale bars 5 µm.

B. Mean intensity of Whi3-tomato is higher in tip droplets (green) than perinuclear droplets (pink).

C. Rate of Whi3 incorporation is higher in tip compared to perinuclear droplets.

D. smFISH images show *BNI1* (green) and *CLN3* (pink) mRNAs are spatially distinct. Nuclei are in blue. Scale bar 5 µm.

E. smFISH images show *BNI1* (green) mRNAs co-localize with polarity mRNA *SPA2* (pink). Nuclei are in blue. The green arrow marks where the RNAs overlap at the tip. Inset scale bar 2 µm.

F. *BNI1* and *SPA2* are significantly more co-localized than *BNI1* and *CLN3*. $p<0.001$ for tips and $p<0.01$ for nuclei (Fisher's Exact test). n= 40 nuclei and tips for $\geq$30 cells.
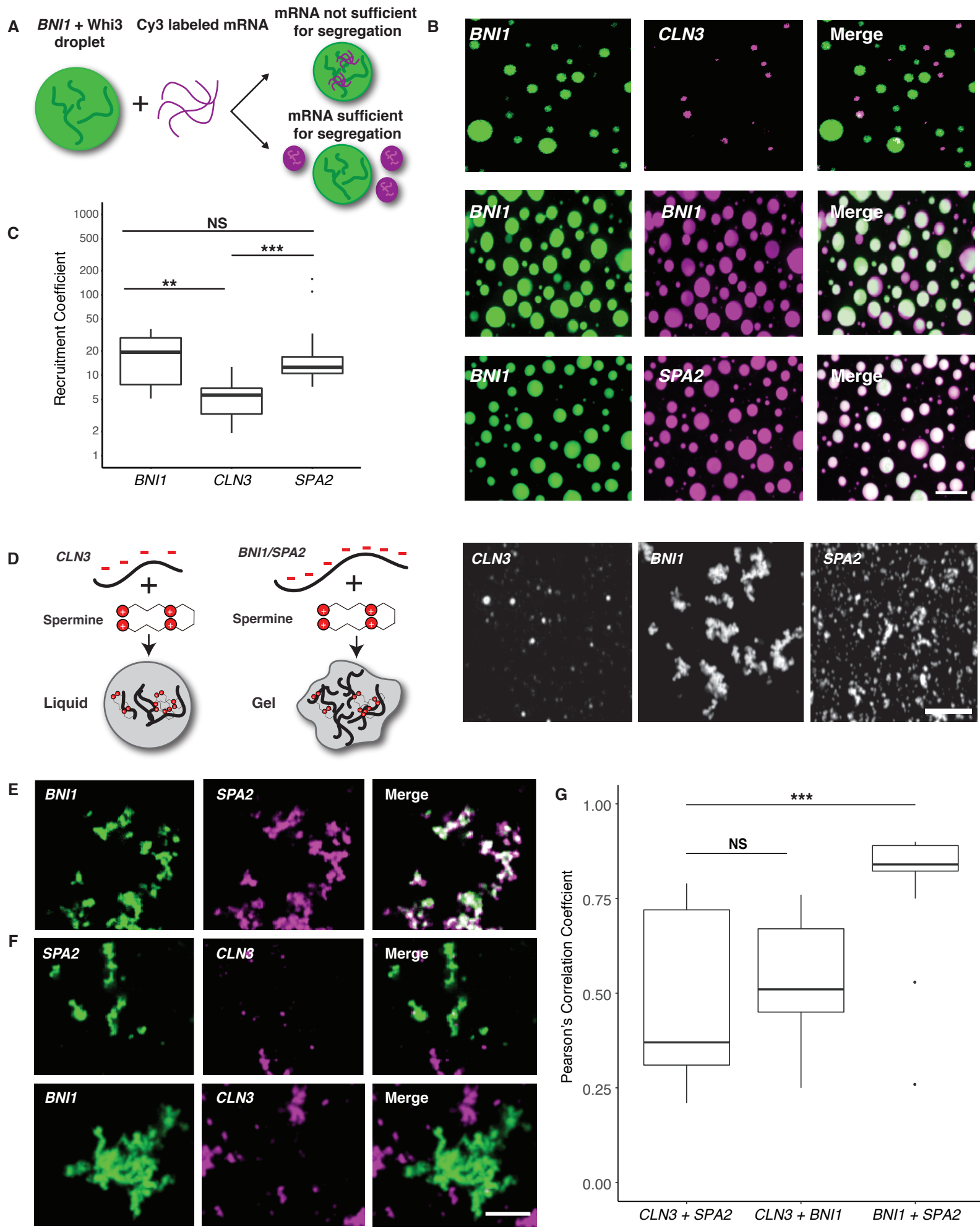
Figure 2 Langdon et al.

A *BNI1* + Whi3 droplet — Cy3 labeled mRNA — mRNA not sufficient for segregation / mRNA sufficient for segregation

B *BNI1* / *CLN3* / Merge ; *BNI1* / *BNI1* / Merge ; *BNI1* / *SPA2* / Merge

C Recruitment Coefficient — NS, ***, ** — *BNI1*, *CLN3*, *SPA2*

D *CLN3* + Spermine → Liquid ; *BNI1/SPA2* + Spermine → Gel ; *CLN3* / *BNI1* / *SPA2*

E *BNI1* / *SPA2* / Merge

F *SPA2* / *CLN3* / Merge ; *BNI1* / *CLN3* / Merge

G Pearson's Correlation Coefficient — NS, *** — *CLN3 + SPA2*, *CLN3 + BNI1*, *BNI1 + SPA2*

Figure 2. Polarity and cyclin complexes segregate *in vitro*.

A. Experimental schematic of in vitro droplet recruitment assay.

B. *CLN3* mRNA (pink) is not efficiently recruited but *BNI1* or *SPA2* mRNA (pink) are recruited into preformed Whi3-*BNI1* droplets (green) based on fluorescence microscopy. Scale bar 10 μm.

C. Recruitment coefficients of mRNA from **B**. Boxes indicate interquartile range, line is median and whiskers contain points within three times the interquartile range, and outliers are indicated with (•) marks. NS, not significant, $p > 0.05$; **, $p < 0.01$; ***, $p < 0.001$ (t test). n ≥500 droplets for N≥3 biological replicates.

D. Cartoon schematic and representative images showing *in vitro* RNA-only droplet assay where *CLN3*, *BNI1*, and *SPA2* mRNAs assemble into liquid or gel-like droplets. Scale bar 5 μm.

E. Fluorescence microscopy images showing *BNI1* RNA (green) colocalizes with SPA2 RNA (pink) in droplets.

F. Fluorescence microscopy images showing *CLN3* RNA (pink) does not colocalize with *SPA2* (green) and *BNI1* (green) droplets. Scale bar 5 μm.

G. Quantification of co-localization between *BNI1* and *SPA2, SPA2* and *CLN3,* or *BNI1* and *CLN3* RNAs. NS, not significant, ***, $p < 0.001$ (Wilcoxon rank-sum test). n≥200 droplets for N≥3 biological replicates.
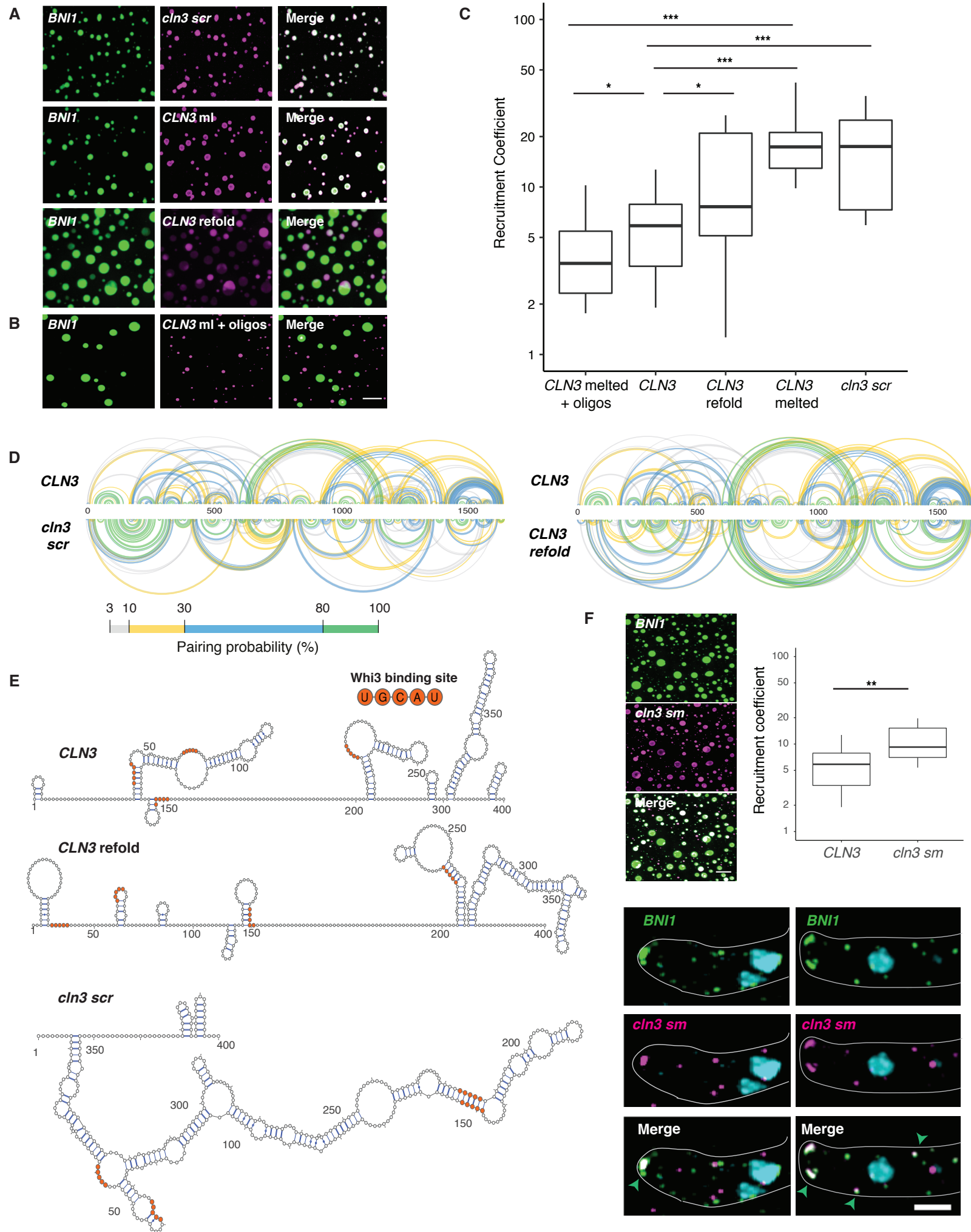
Figure 3 Langdon et al.

Figure 3. RNA secondary structure determines specificity and identity of Whi3-*CLN3* droplets.

A. Fluorescence microscopy images showing the recruitment of scrambled (*cln3 scr*), melted (*CLN3* ml), and refolded *CLN3* (*CLN3* refold) mRNA (pink) into preformed Whi3-*BNI1* droplets (green).

B. Fluorescence microscopy images showing the loss of recruitment of *CLN3* ml when mixed with oligonucleotides targeting complementary sequences of *CLN3* to *BNI1*. Scale bar 10 μm.

C. Quantification of **A** and **B**. *, $p<0.05$; **, $p<0.01$; ***, $p < 0.001$ (t test). $n \geq 500$ droplets for $N \geq 3$ biological replicates.

D. Base pairing probability from SHAPE-MaP of *CLN3*, *cln3 scr*, and *CLN3* refold show differences in the secondary structure in *CLN3*. Arcs connect base pairs and are colored by probability.

E. Secondary structure models from SHAPE-MaP for the first 400 nucleotides of *CLN3*, *CLN3* refold, and *cln3 scr*. Whi3 binding sites are in orange.

F. *CLN3* structure mutant (*cln3 sm*) mRNA is significantly recruited to Whi3-*BNI1* droplets *in vitro* and *in vivo*. **, $p<0.01$ (t test). Green arrows denote sites of co-localization between *BNI1* mRNA (green) and *cln3 sm* mRNA (pink) by smFISH. Scale bar 10 μm for *in vitro*, 2 μm for *in vivo*. $n \geq 500$ droplets for $N \geq 3$ biological replicates.
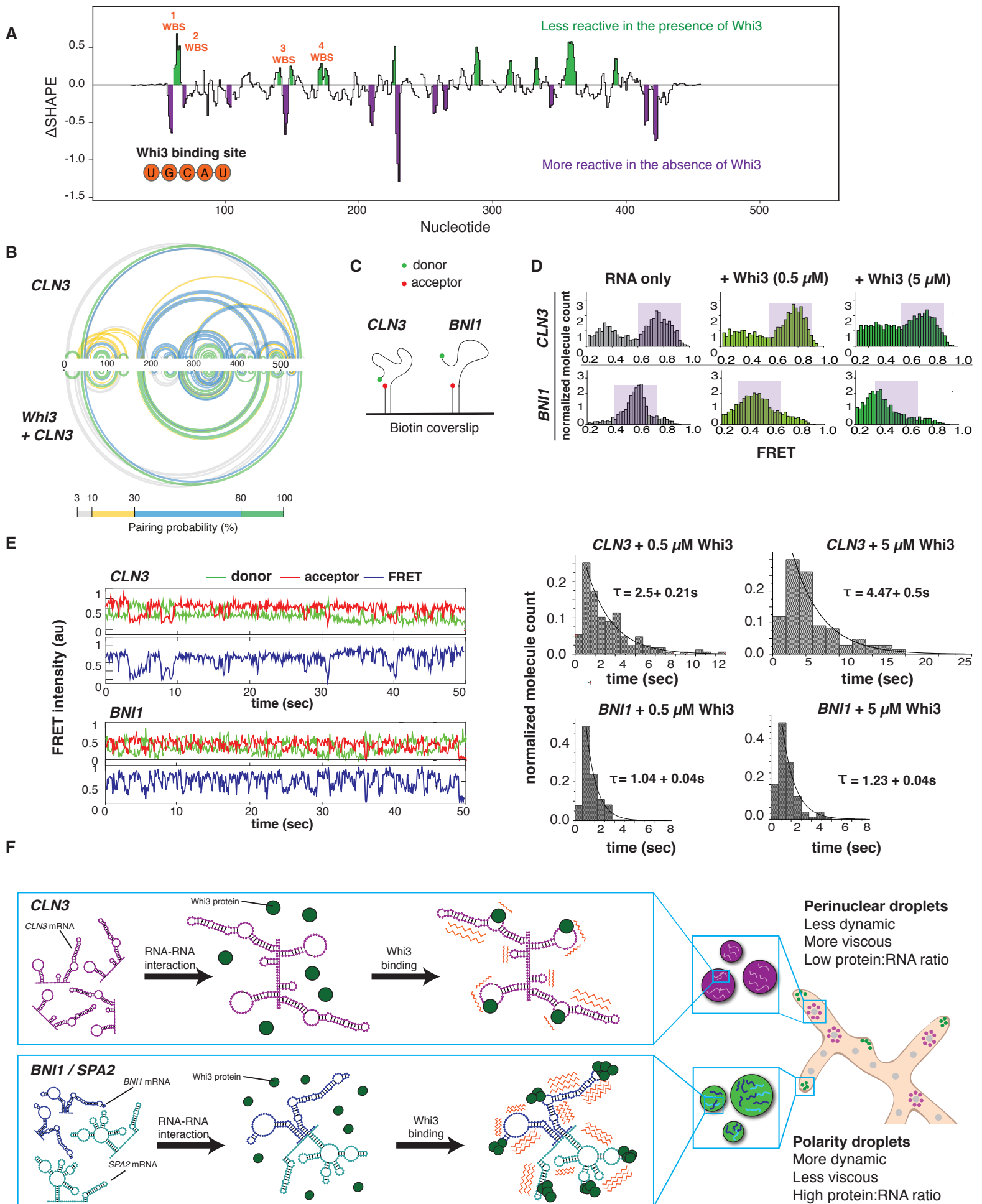
Figure 4 Langdon et al.

A — ΔSHAPE plot. Labels: WBS 1, WBS 2, WBS 3, WBS 4. "Less reactive in the presence of Whi3" (green). "More reactive in the absence of Whi3" (purple). Whi3 binding site: U G C A U. X-axis: Nucleotide (100–500). Y-axis: ΔSHAPE (0.5 to −1.5).

B — CLN3, Whi3 + CLN3. Pairing probability (%): 3, 10, 30, 80, 100.

C — donor (green), acceptor (red). CLN3, BNI1. Biotin coverslip.

D — RNA only, + Whi3 (0.5 μM), + Whi3 (5 μM). CLN3, BNI1. normalized molecule count vs FRET.

E — CLN3: donor, acceptor, FRET. BNI1. FRET intensity (au) vs time (sec).
CLN3 + 0.5 μM Whi3: τ = 2.5 + 0.21s
CLN3 + 5 μM Whi3: τ = 4.47 + 0.5s
BNI1 + 0.5 μM Whi3: τ = 1.04 + 0.04s
BNI1 + 5 μM Whi3: τ = 1.23 + 0.04s

F — CLN3: CLN3 mRNA, Whi3 protein, RNA-RNA interaction, Whi3 binding. Perinuclear droplets: Less dynamic, More viscous, Low protein:RNA ratio.
BNI1 / SPA2: BNI1 mRNA, SPA2 mRNA, Whi3 protein, RNA-RNA interaction, Whi3 binding. Polarity droplets: More dynamic, Less viscous, High protein:RNA ratio.

Figure 4. Whi3 binding alters RNA behavior.

A. Differences in SHAPE reactivities (ΔSHAPE) were calculated by subtracting *CLN3* SHAPE reactivities from *CLN3* + Whi3 reactivities. Positive ΔSHAPE values indicate protection from modification in the presence of Whi3 and negative ΔSHAPE reports enhanced reactivity in the absence of Whi3 protein.

B. Base pairing probability compared between *CLN3* and *CLN3* with Whi3 shows rearrangements in *CLN3* structure in the presence of Whi3. Arcs connect base pairing sites and are colored by probability.

C. Schematic of smFRET experiment.

D. FRET histograms before (gray) and after (green) 0.5 or 5 µM Whi3 addition. Purple shaded regions denote high and mid FRET states for *CLN3* and *BNI1*, respectively.

E. Averaged cy3 (green), cy5 (red) intensities, and representative FRET traces (blue) obtained from smFRET experiments of *CLN3* and *BNI1* in the presence of 5 µM Whi3. Dwell time analysis reveals slower FRET fluctuations for *CLN3* than *BNI1* in the presence of Whi3.

F. Proposed model in which RNA-RNA interactions derived from mRNA structure promotes the selective uptake of distinct RNAs and protein constituents into droplets leading to distinct dynamics (orange zigzags) of different droplet complexes.

Supplemental Figure 1 Langdon et al.

A

Whi3

N [============== polyQ | RRM ==] C

QQQQLQQQQHHLQQQQHQQQQQSLS
QQPQQQQSQQSQAHSQQHQQQHQQQ
QQQQQPQQQQPQQHPPQQPQQQNSQ
QAIVGQSQQQVTSGQQK

B
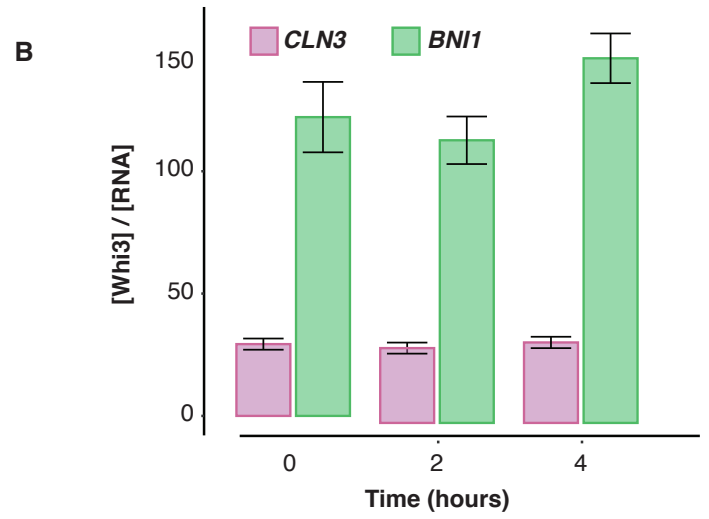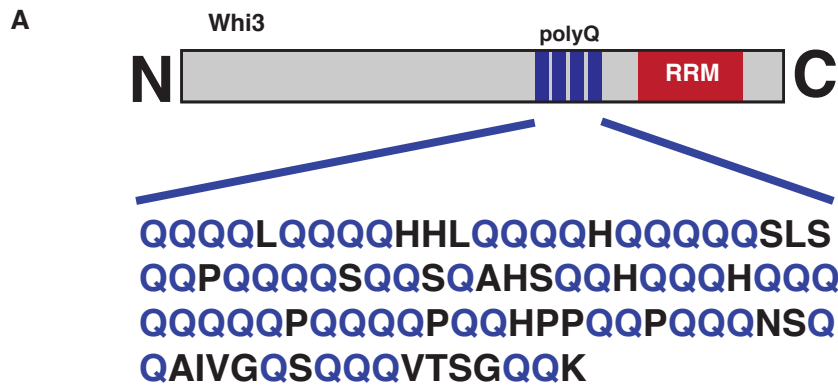

C

D

E
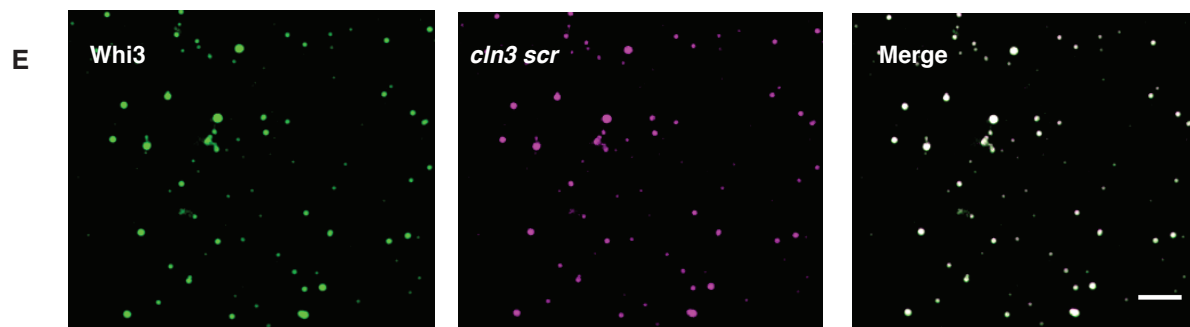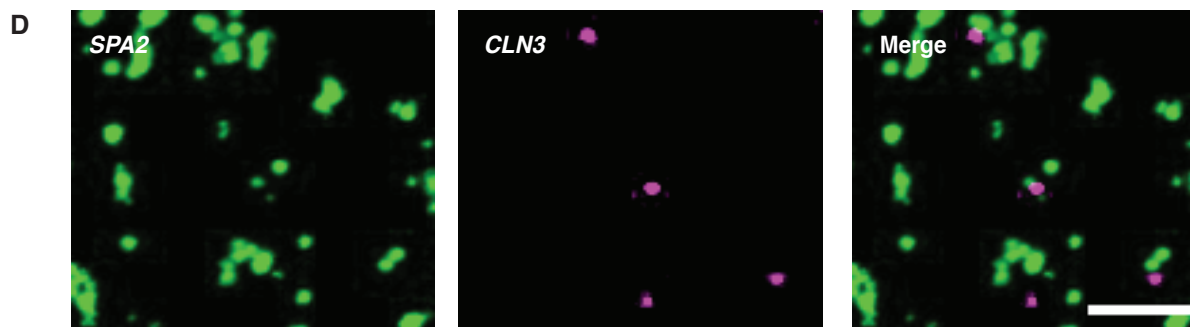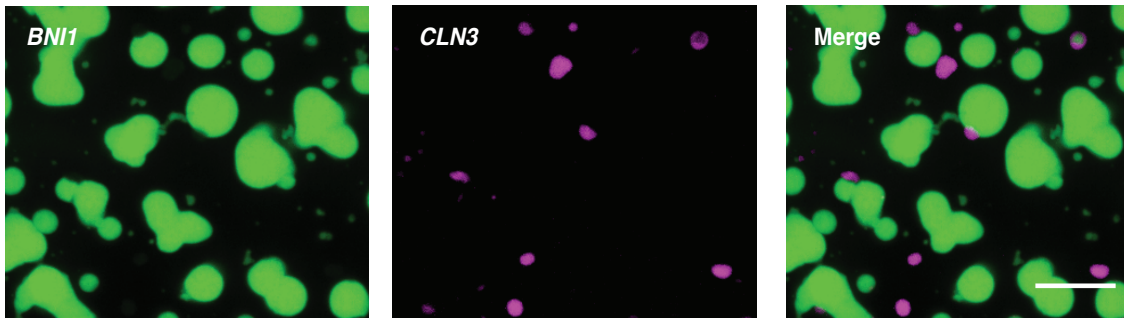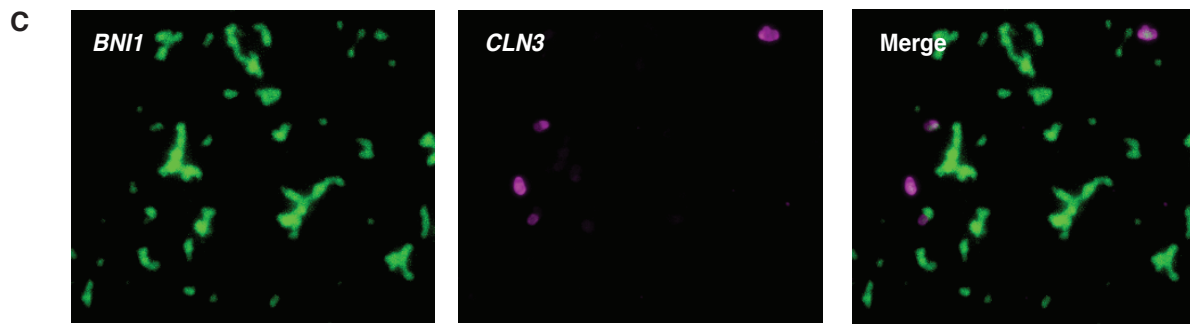
Fig. S1. Whi3, a polyQ-containing protein, forms LLPS droplets *in vitro*.

A. Cartoon schematic of Whi3 protein sequence, in *A. gossypii*, depicting the disordered (polyQ, blue) and RNA binding domains (RRM, red).

B. Whi3-*BNI1* droplets (green) incorporate more Whi3 protein over time *in vitro* compared to Whi3-*CLN3* droplets (pink). Data are mean ± SD. n ≥ 100 droplets for N= 2 biological replicates.

C. Fluorescence microscopy images showing *CLN3* (pink*)* is excluded from Whi3-*BNI1* (green) droplets in a variety of protein and RNA concentrations. Top, Whi3 2 µM, RNA 1.25 nM; Bottom, Whi3 20 µM, RNA 5 nM. Scale bar is 10 µm.

D. Fluorescence microscopy images show cy3 labeled *CLN3* mRNA (pink) is not efficiently recruited into Whi3-*SPA2* droplets (green) (8 µM Whi3, 5 nM RNA) Images are representative of observations from three independent experiments. Scale bar is 10 µm.

E. Fluorescence microscopy images showing the recruitment of *cln3 scrambled* mRNA (5 nM, pink) into droplets with Whi3 (8 µM, green). Scale bar is 10 µm.
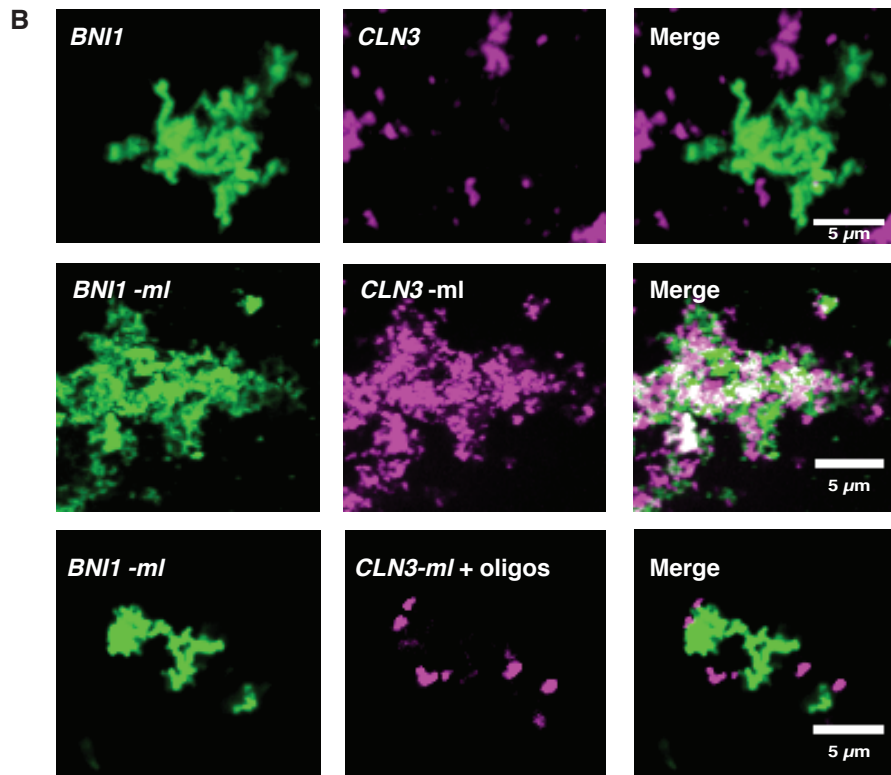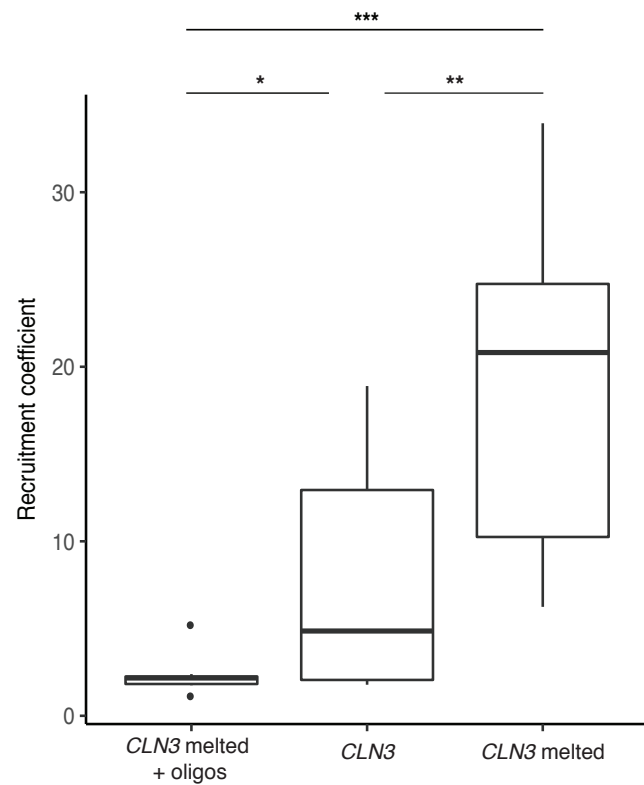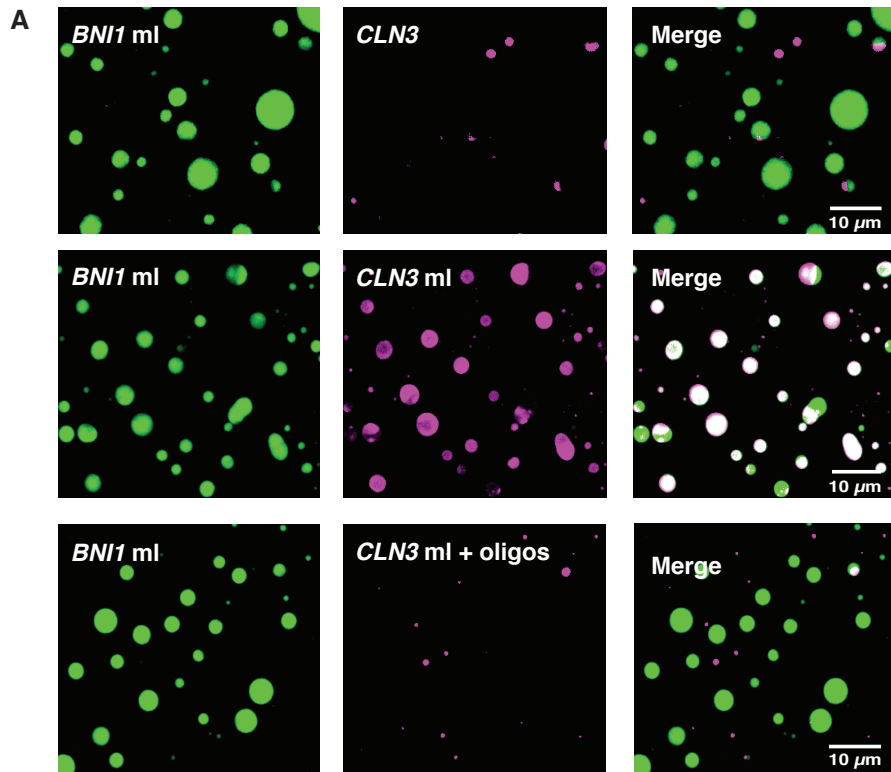
Supplemental Figure 2 Langdon et al.
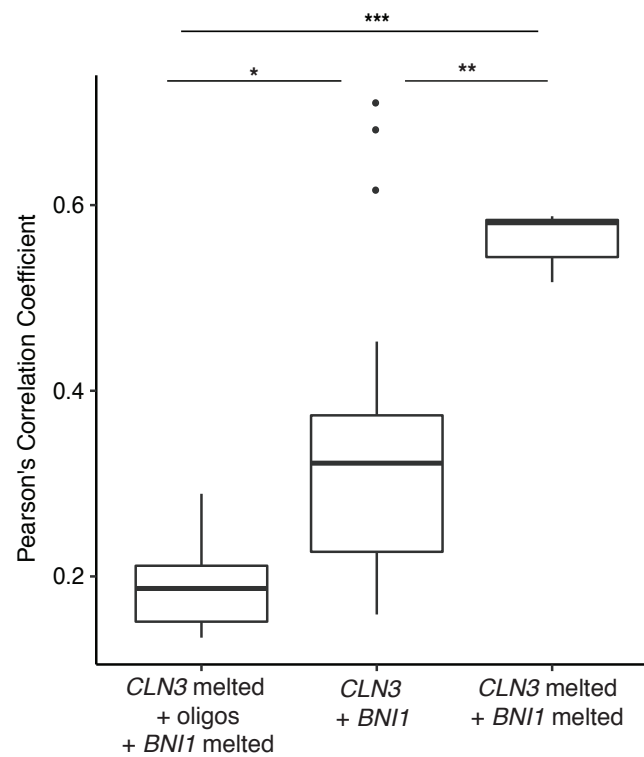
Fig. S2. *CLN3* and *BNI1* **co-assemble when regions of complementarity between the two RNAs are exposed through melting.**

A. Fluorescence microscopy images and recruitment coefficients show *CLN3* mRNA (5 nM, pink) is modestly recruited into preformed Whi3 droplets made with melted *BNI1* (8 µM Whi3, 5 nM *BNI1*, green) unless complement regions of *CLN3* are also exposed through melting (*CLN3* ml). In contrast, recruitment of *CLN3* ml is lost when the mRNA is mixed with oligos targeting the sequence on *CLN3* with complementarity to *BNI1* mRNA (*CLN3* ml + oligos). Outliers are indicated with (•) marks. *, $p < 0.05$; **, $p < 0.01$; ***, $p < 0.001$ (unpaired t test). $n \geq 500$ droplets for $N \geq 3$ biological replicates.

B. Fluorescence microscopy images and quantification (Pearson's correlation coefficient) show *CLN3* (10 nM, pink) RNA only droplets colocalize with *BNI1* (10 nM, green) droplets only when melted (*CLN3* ml) and recruitment is lost when the mRNA is mixed with oligos targeting the sequence on *CLN3* with complementarity to *BNI1* mRNA (*CLN3* ml + oligos) Outliers are indicated with (•) marks. *, $p<0.05$, **, $p < 0.01$; ***, $p < 0.001$ as determined by Wilcoxon rank-sum test. $n \geq 200$ droplets for $N \geq 3$ biological replicates.
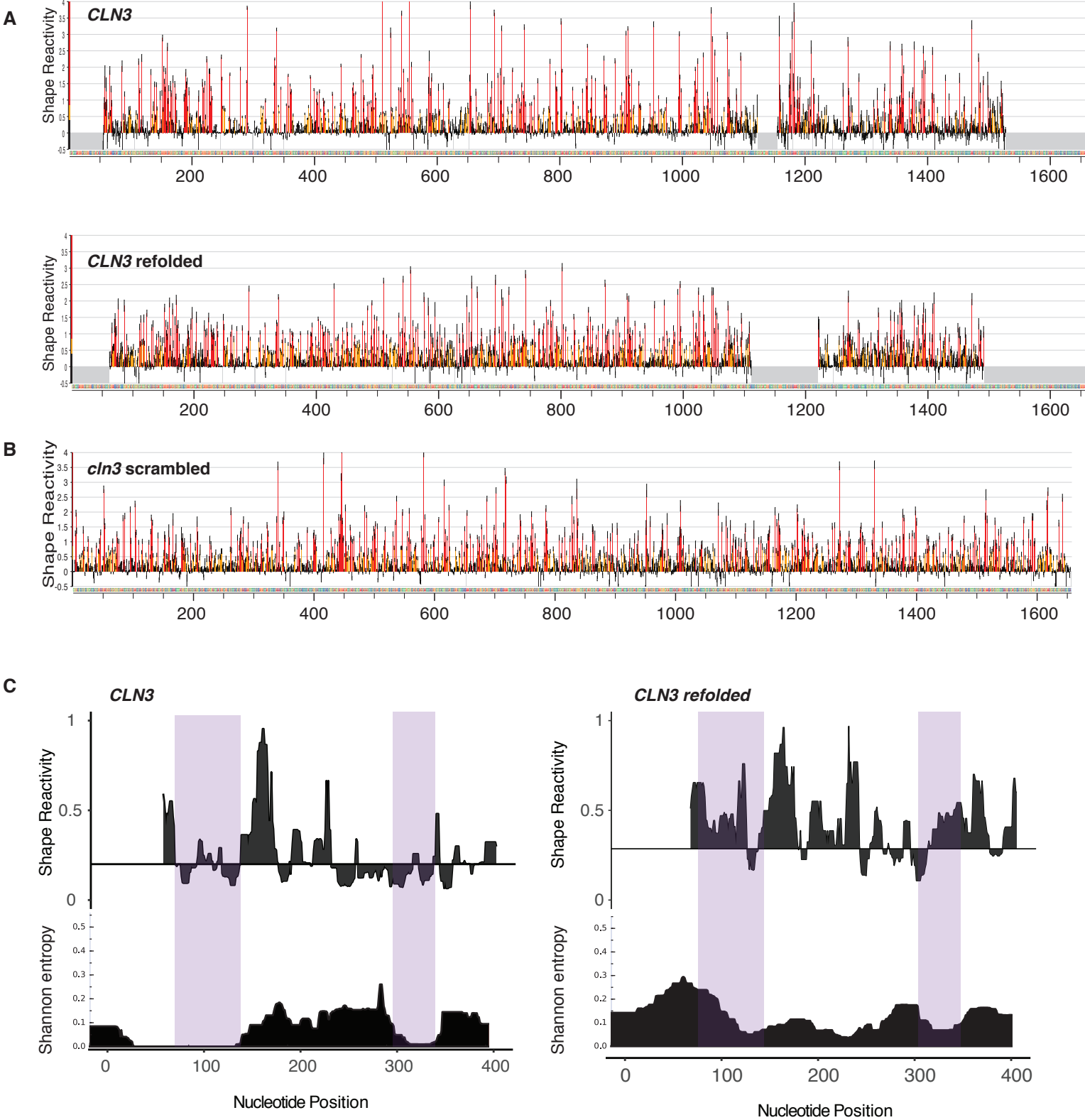
Supplemental Figure 3 Langdon et al.

Fig. S3. *CLN3* mRNA secondary structure is altered when the mRNA sequence is scrambled or refolded.

A. SHAPE reactivity profiles for *CLN3* and *CLN3* refolded. High values indicate unstructured regions or many possible structures, while low values suggest a single well-defined structure. Data are mean ± SD

B. SHAPE reactivity profiles for *cln3 scr* indicates it has a completely different secondary structure than *CLN3* native sequence. Data are mean ± SD.

C. SHAPE reactivity and Shannon entropy values for the first 400 nucleotides of the RNAs shown as the median reactivity smoothed over a 19-nt sliding window relative to the global median. Reactivity values for *CLN3* in this region are significantly lower than reactivity values for *CLN3* refolded (median of 0.19 vs 0.32 respectively; Wilcoxon rank sum test, $p = 0.001$), suggesting that the *CLN3* refolded mRNA contains less well-defined structures. Purple shaded regions show low-SHAPE/low-entropy regions. These regions transition to high-SHAPE/high-entropy regions when the *CLN3* sequence is melted and refolded.
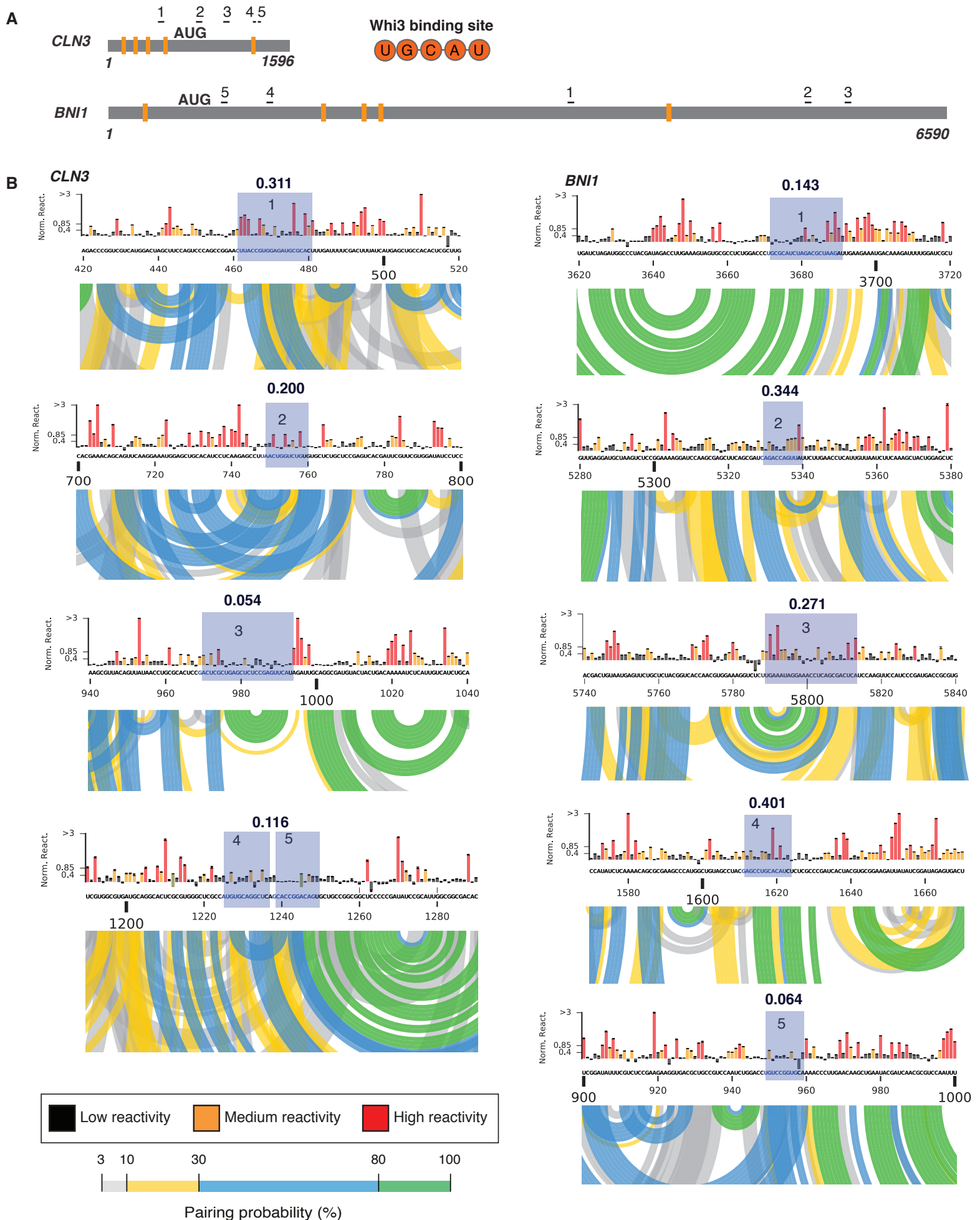
Supplemental Figure 4 Langdon et al.

A

CLN3

Whi3 binding site

U G C A U

BNI1

B *CLN3*   *BNI1*

Low reactivity   Medium reactivity   High reactivity

Pairing probability (%)

Fig. S4. Regions of Complementarity between *CLN3* and *BNI1*.

A. Cartoon schematic of *CLN3* and *BNI1* RNA depicting the location of Whi3 binding sites (orange) and the regions of complementarity (numbered) between the two RNAs. RNAs are drawn to scale.

B. Shape reactivity and arc plots for the five regions along *CLN3* that can base-pair with *BNI1* and regions on *BNI1* that can base pair with *CLN3*. The blue shaded regions indicate the exact complement sequence. Most of these regions on both *CLN3* and *BNI1* are located in low SHAPE, high structured regions, indicating that these regions are likely not exposed and unable to interact when properly folded. The median SHAPE reactivity per region is displayed above its respective region. Data are mean ± SD.
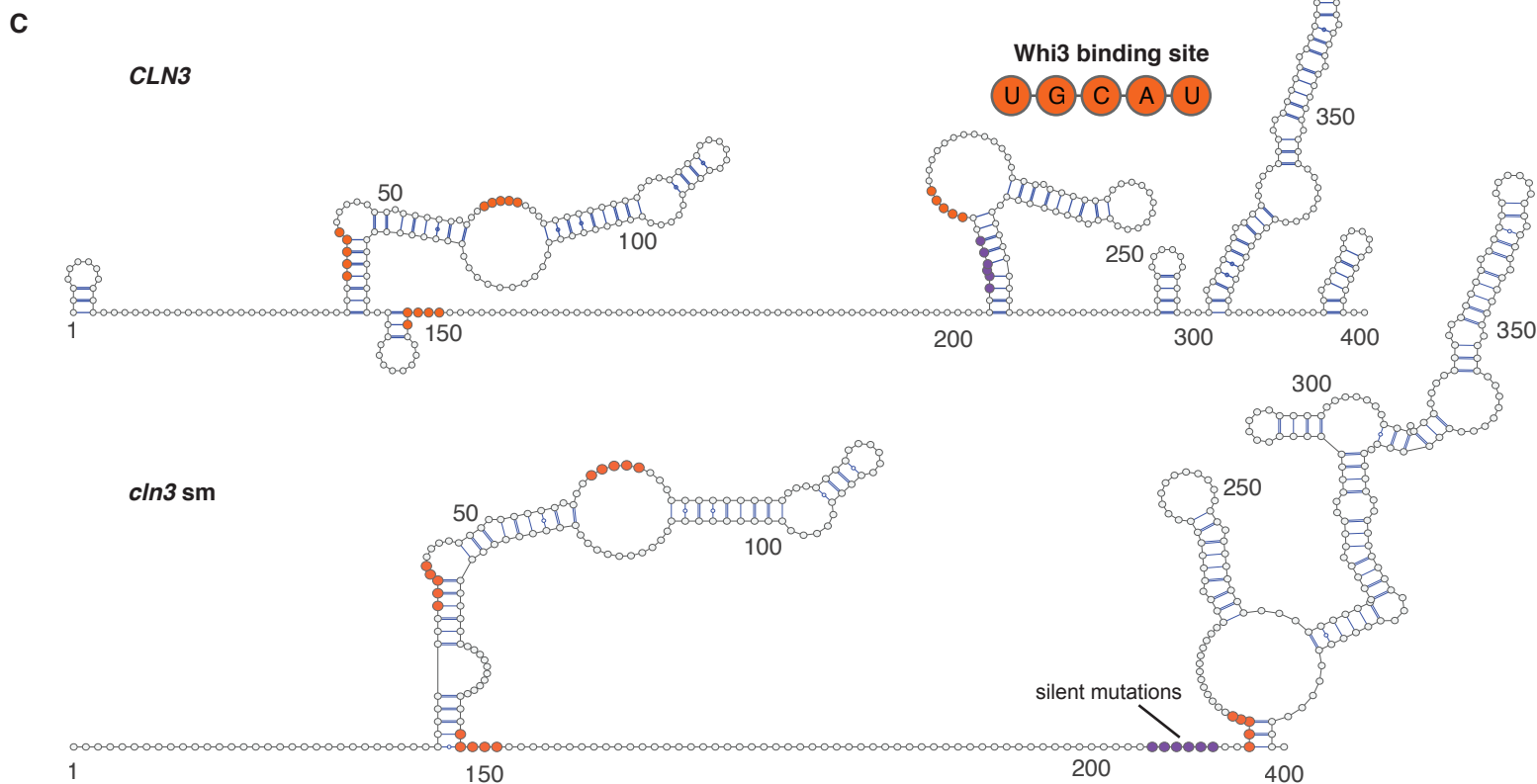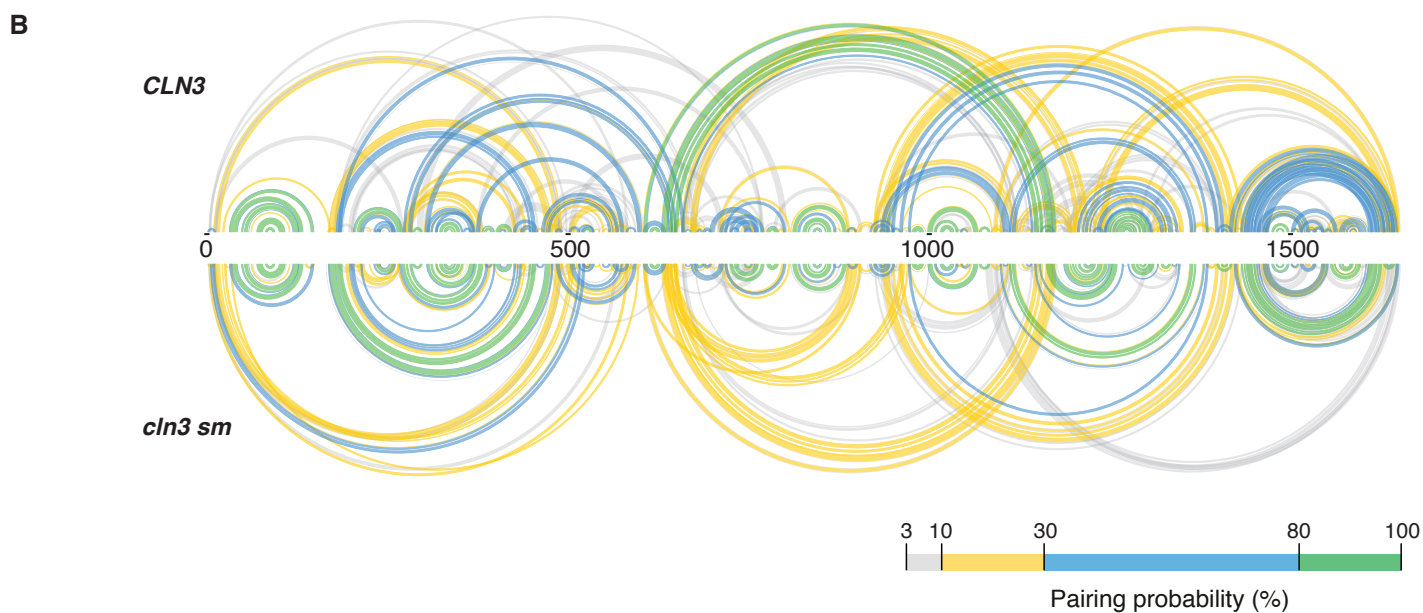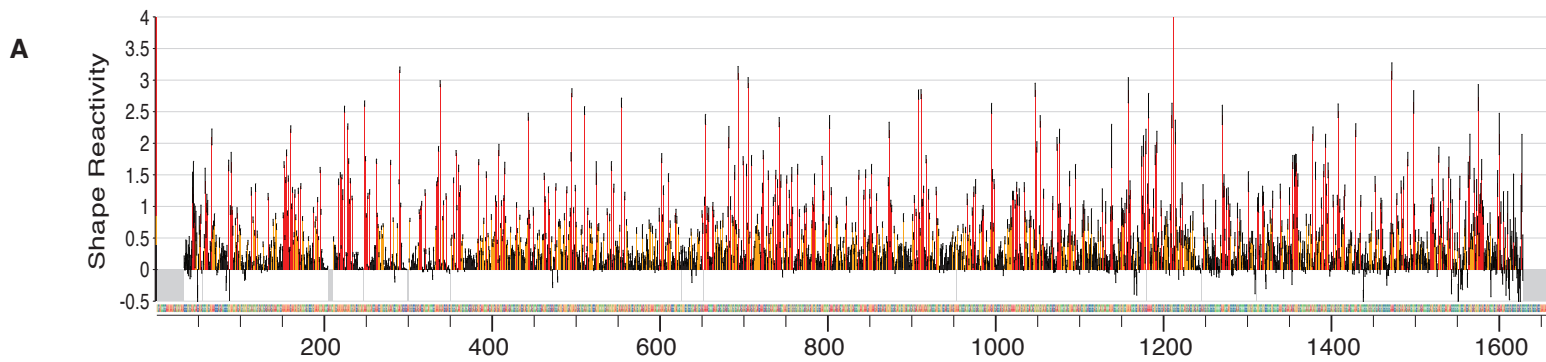
Supplemental Figure 5 Langdon et al.

Fig. S5. *CLN3* **mRNA secondary structure is altered with point mutations to target stem loops.**

A. Shape reactivity profiles for *CLN3* structure mutant *(cln3 sm)*. High values indicate unstructured regions or many possible structures, while low values suggest a single well-defined structure. Data are mean ± SD.

B. Base pairing probability compared among *CLN3* and *cln3 sm* show differences in the secondary structure between the two mRNAs. Arcs connect base pairs and are color coded by probability.

C. Secondary structure models for the first 400 nucleotides of *CLN3* and *cln3 sm*. Whi3 binding sites are denoted in orange. The sequence targeted for mutation in *cln3 sm* is denoted in purple.
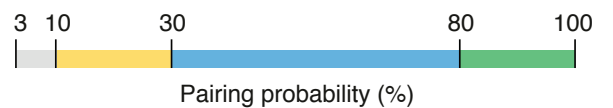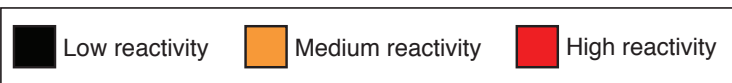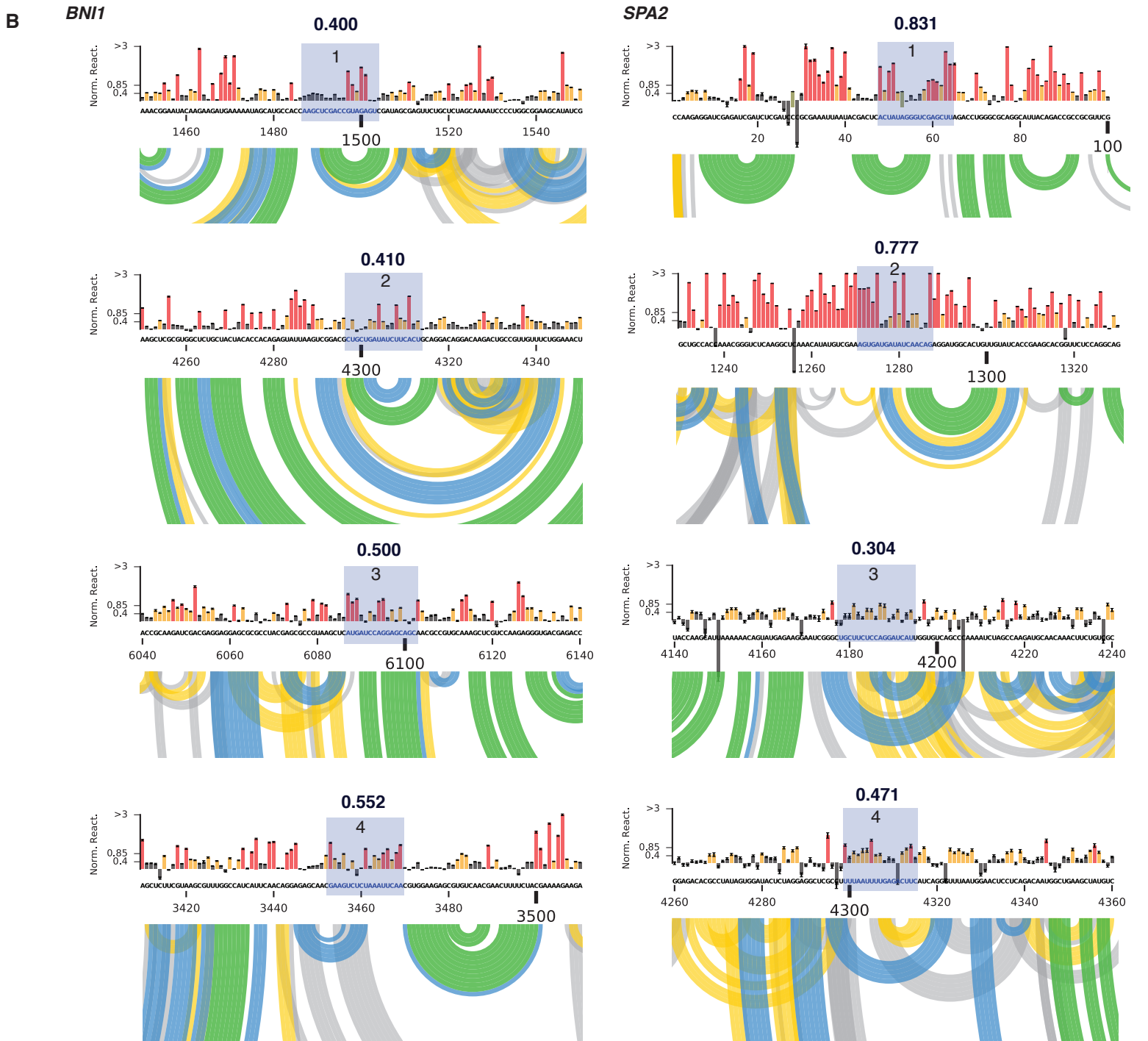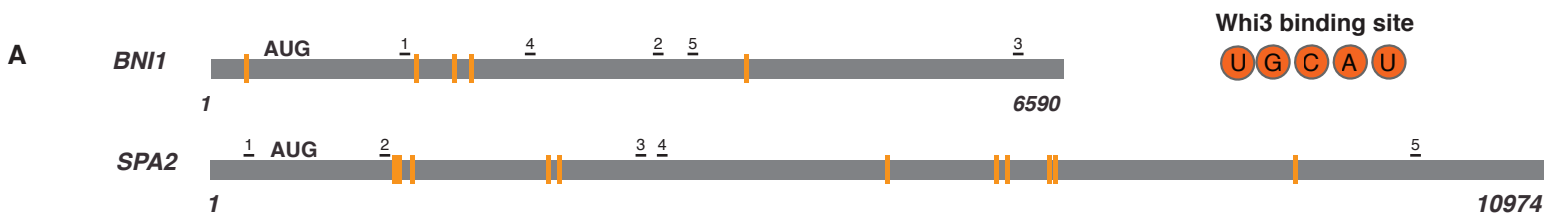
Supplemental Figure 6 Langdon et al.

A

BNI1

SPA2

Whi3 binding site

U G C A U

B

BNI1

SPA2

Low reactivity   Medium reactivity   High reactivity

3 10   30   80   100

Pairing probability (%)

Fig. S6. Regions of complementarity between *BNI1* and *SPA2*.

A. Cartoon schematic of *BNI1* and *SPA2* RNA depicting the location of Whi3 binding sites (orange) and the regions of complementarity between the two RNAs. RNAs are drawn to scale.

B. Shape reactivity and arc plots for the five regions along *BNI1* that can base-pair with *SPA2* and regions on *SPA2* that can base pair with *BNI1*. The blue shaded regions indicate the exact complement sequence. Most of these regions are located in high SHAPE, low structured regions, indicating that these regions are likely exposed and able to interact. The median SHAPE reactivity per region is displayed above its respective region. Data are mean ± SD.

Supplemental Figure 7 Langdon et al.
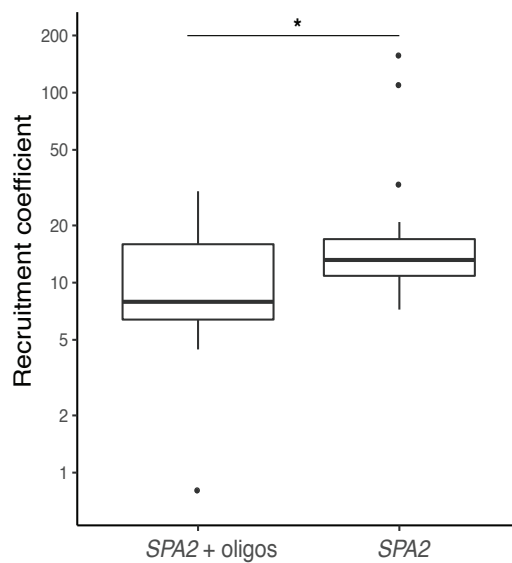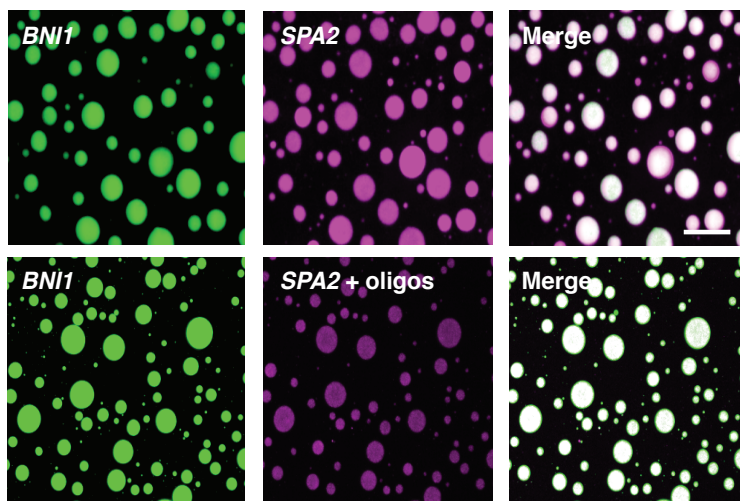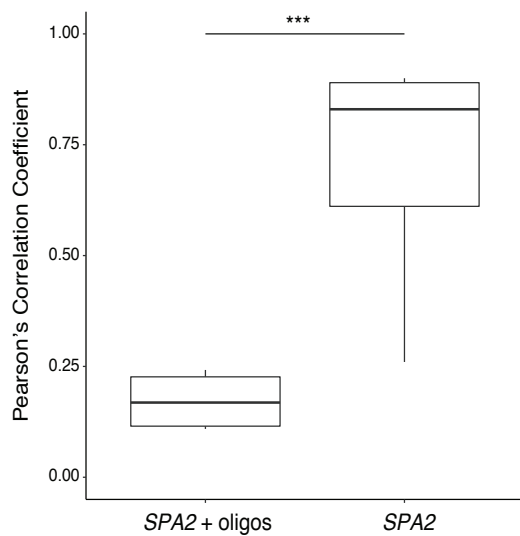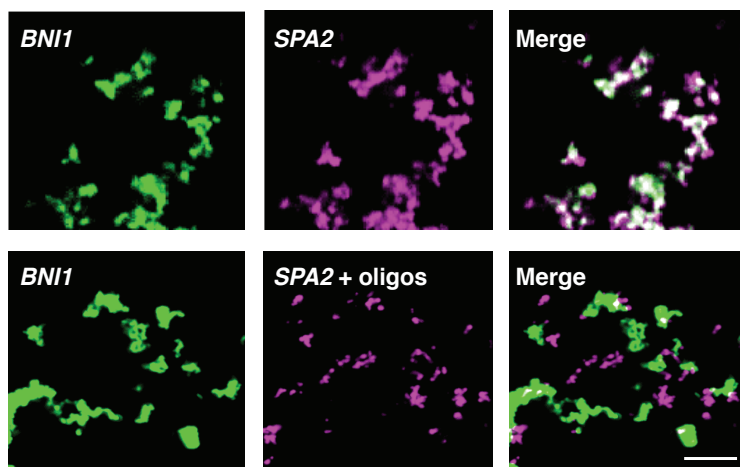
Fig. S7. Disruption of regions of complementarity interferes with coassembly between two RNAs.

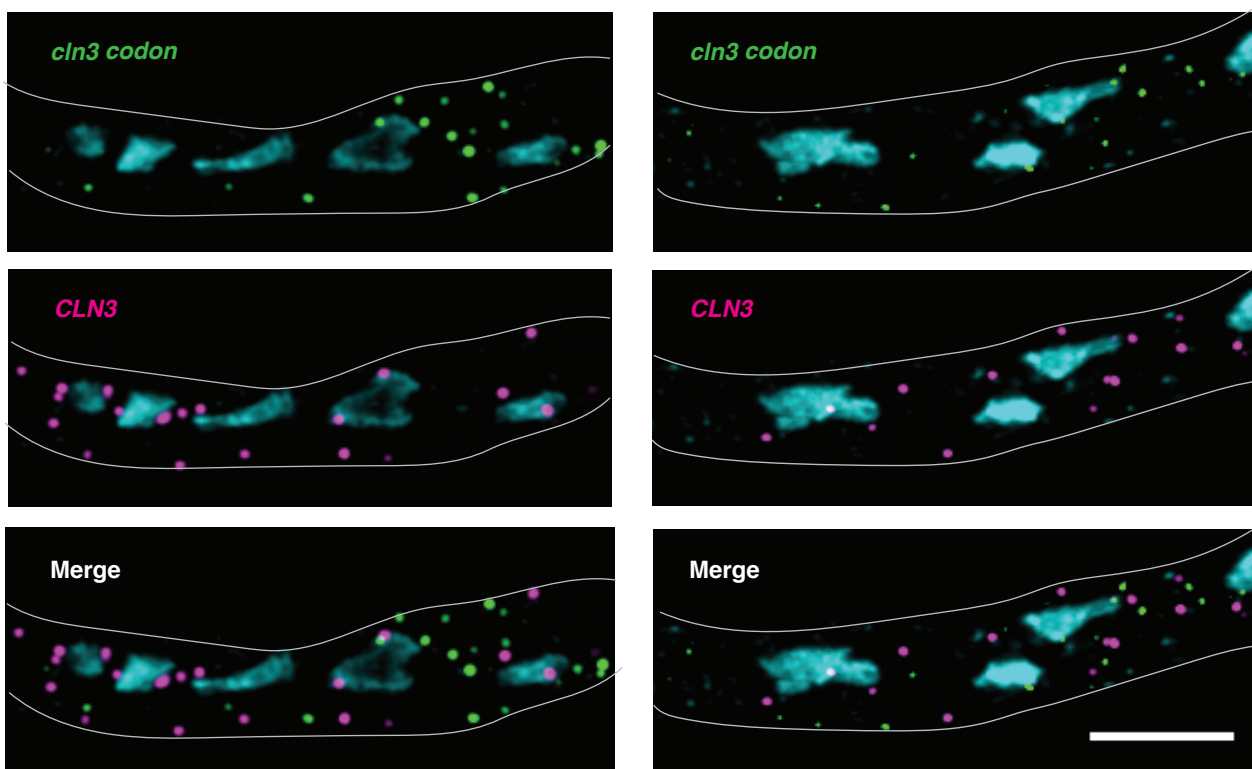**A.** Fluorescence microscopy images and quantification show *SPA2* mRNA incubated with oligos to target the complement nucleotide regions of *BNI1* (5 nM, pink) is less recruited into preformed Whi3-*BNI1* droplets (8 μM Whi3, 5 nM *BNI1*, green) compared to native *SPA2* alone. The line at the center of the box indicates the median value, and boxes indicate interquartile range. Whiskers contain data points within 3 times the interquartile range, and outliers are indicated with (•) marks. *, $p < 0.05$ (unpaired t test). Scale bar is 10 μm. n≥500 droplets for N≥ 3 biological replicates.

B. Fluorescence microscopy images and quantification (Pearson's correlation coefficient) showing *SPA2* mRNA (10 nM, pink) incubated with oligos to target the complement nucleotide regions to *BNI1* (5 nM, pink) are excluded from *BNI1* mRNA (10 nM, green) in the presence of Spermine. ***, $p < 0.001$ (Wilcoxon rank-sum test). Scale bar is 5 μm. n≥200 droplets for N≥ 3 biological replicates.

C. Single molecule mRNA FISH images show that a codon randomized *CLN3* (*cln3 codon*, green) mRNA does not co-localize with endogenous *CLN3* mRNA (pink) *in vivo*. Scale bar is 5 μm.

Supplemental Figure 8 Langdon et al.

Fig. S8. Whi3 binding sites are located in highly structured region along *BNI1* mRNA.

A. Cartoon schematic of *BNI1* RNA depicting the location of the five Whi3 binding sites (orange). RNA is drawn to scale.

B. Secondary structure plots show regions of *BNI1* mRNA surrounding Whi3 binding sites.

Supplemental Figure 9 Langdon et al.

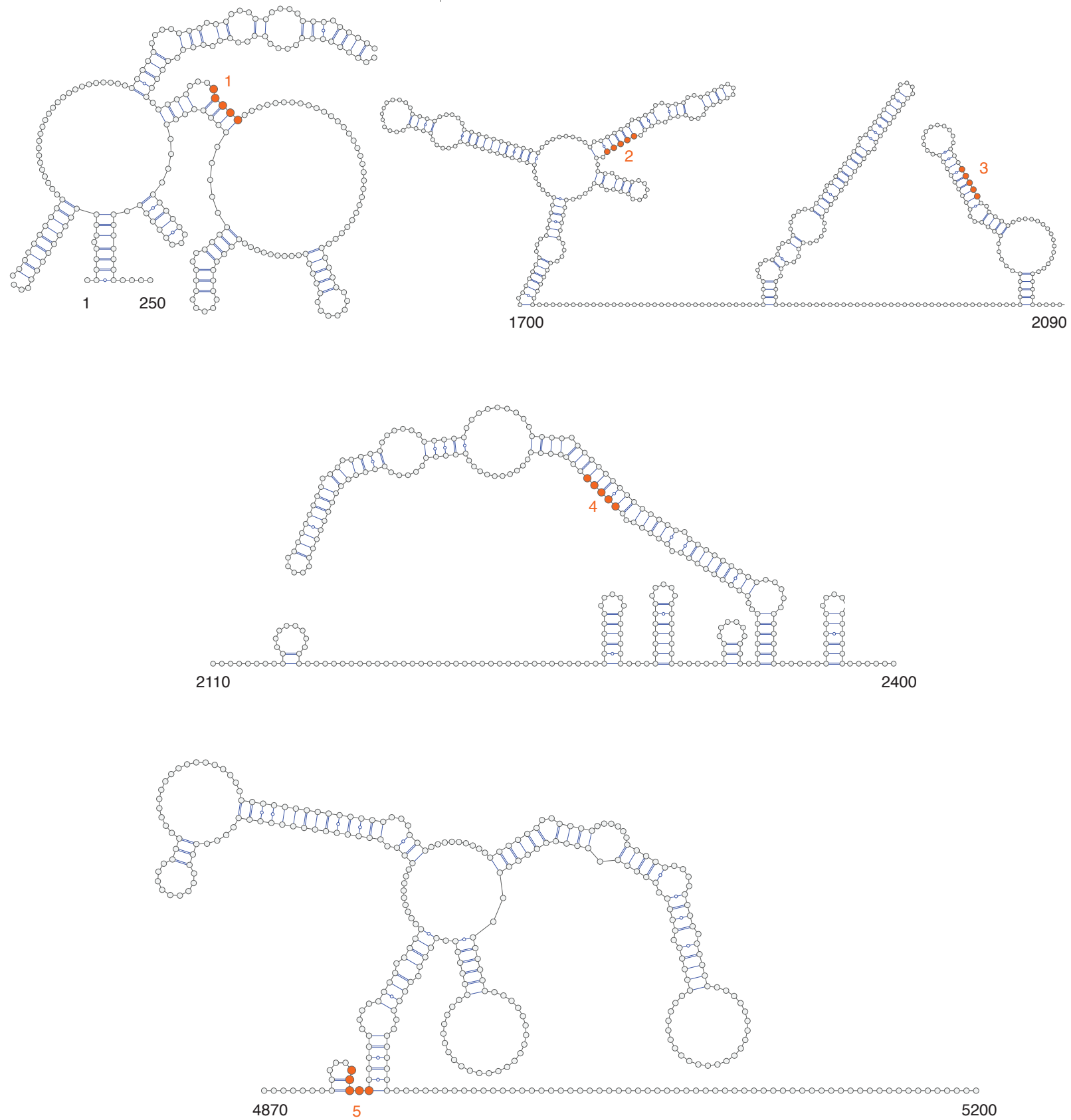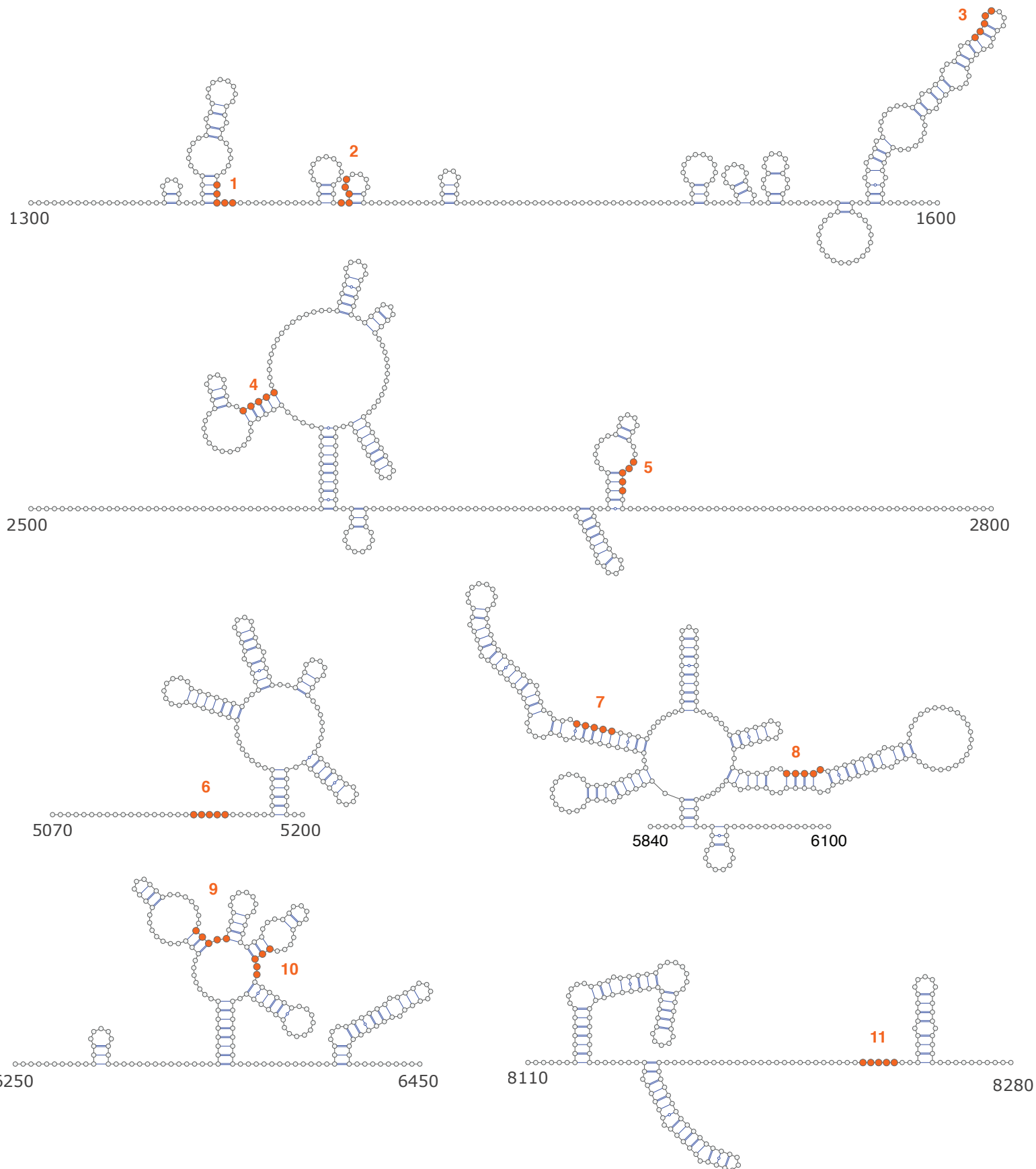**Whi3 binding site**

U G C A U

Fig. S9. The majority of Whi3 binding sites are located in highly structured region along *SPA2* mRNA.

A. Cartoon schematic of *SPA2* RNA depicting the location of the eleven Whi3 binding sites (orange). RNA is drawn to scale.

B. Secondary structure plots show regions of *SPA2* mRNA surrounding Whi3 binding sites.

Supplemental Figure 10 Langdon et al.
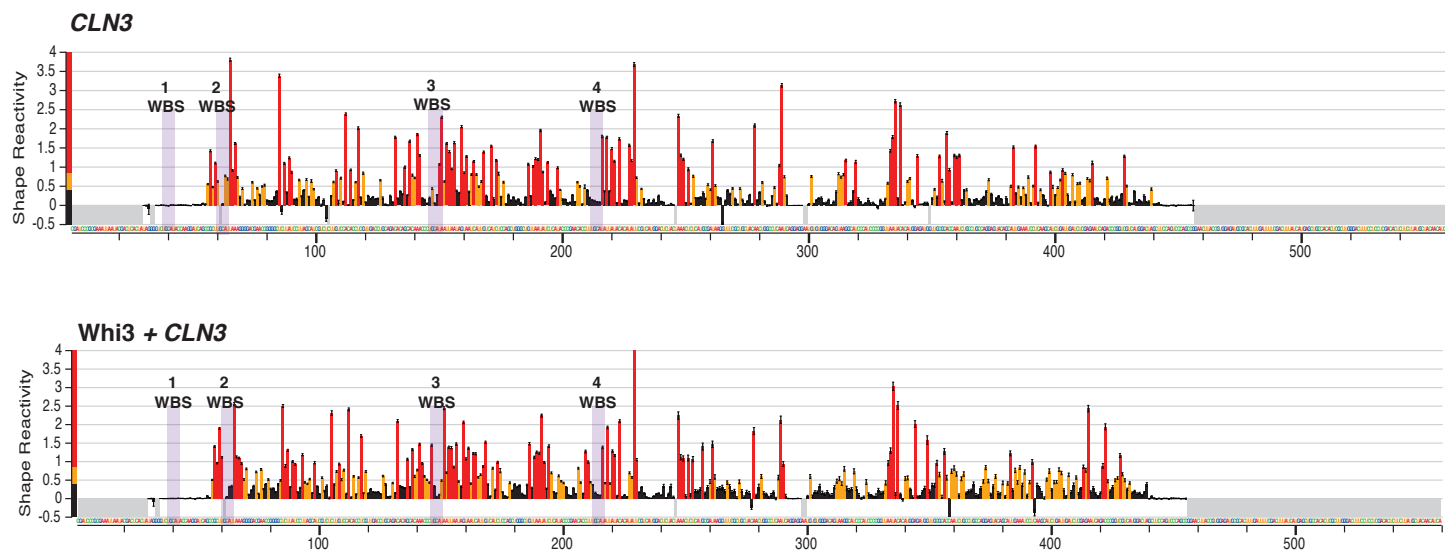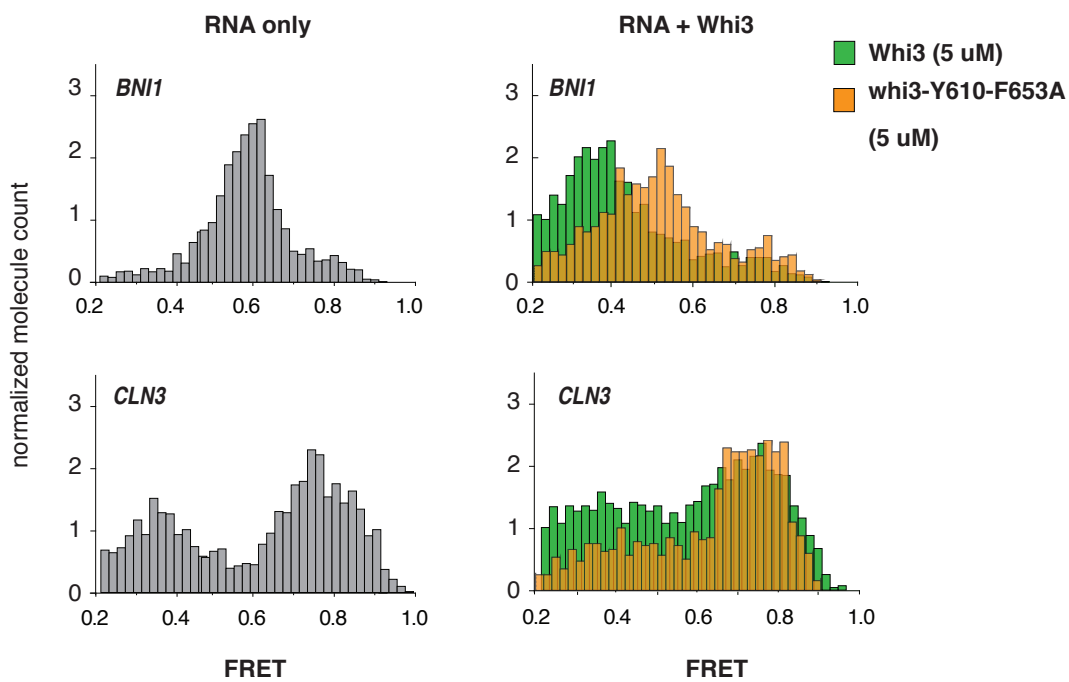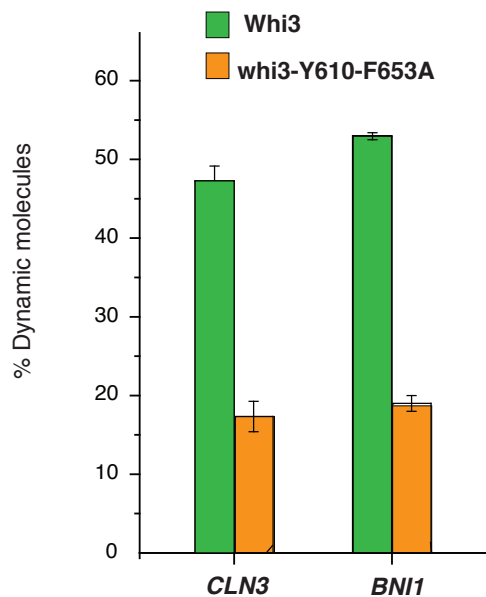
Fig. S10. Whi3 binding is essential to induce dynamic fluctuations to its target mRNAs, *CLN3* and *BNI1*.

A. Shape reactivity profiles for *CLN3* and *CLN3* in the presence of Whi3 protein. High values indicate unstructured regions and many possible structures, while low values suggest a single well-defined structure. The four Whi3 binding sites (WBS) are shaded in purple and show the differences in SHAPE reactivity along *CLN3* in the presence or absence of Whi3. Data are mean ± SD.

B. FRET histograms show RNA only (gray) or addition of Whi3 (green) or a Whi3 RNA binding mutant (whi3-Y610-F653A, orange).

C. The mutant exhibits much lower dynamics with both *CLN3* and *BNI1* indicating that Whi3 binding is needed to induce dynamic fluctuations to the two RNAs.

Materials and Methods

Plasmid and Strain Construction

To create *pcln3sm::GEN*; cln3Δ::NAT1 construct, under the control of its own promoter, the entire plasmid AGB237 (p*CLN3*- GFP::GEN3, AMP) was amplified using primers Phusion polymerase (New England Biolabs) and AGO2308 (GGGCTGTTA ATATCTCATACCCGTTGTGGTTTGCATATTATACACATATTCG) and AGO2309 (CGAATATGTGTATAATATGCAAACCACAACGGGTATGAGATATTAACAGCCC). This mutated a region 31 base pairs upstream of the ORF from AACACC to TTGTGG. The reaction was digested with DpnI (New England Biolabs). The 5'UTR, ORF, and 3'UTR were sequenced by Genewiz, confirming that TTGTGG was the only mutation. This plasmid was transformed into *A. gossypii* AG612 (*cln3Δ::NAT1*) via electroporation and selection on AFM+G418 plates.

To create *pcln3sm::GEN* under control of a T7 promoter, the entire plasmid AGB690 (*CLN3*-GFP) was amplified with the primers AGO2308 and AGO 2309 using the QuickChange XL Site-Directed Mutagenesis kit (Agilent Technologies) following the instructions. The 5'UTR, ORF, and 3'UTR were sequenced by Genewiz, confirming that TTGTGG was the only mutation. This plasmid was then digested and used as a template to transcribe RNA using the T7 HiScribe in vitro transcription kit (NEB).

To create the p*cln3scr2*; ΔlΔt a geneblock containing the scrambled coding sequence for *CLN3* was ordered from GenScript and amplified with primers 5' TAAACGAAG GCAAAGAGCTCGGTACCCGGGGACGTTCACTAATCTTAATACG 3' and 5'GTGAAAAGTTCTTCTCCTTTACTCATCTCAGTACGCGGCCGCTCGAGAGATCTTGT AATTAATCCTGC 3'. AGB392, a plasmid containing GFP under the control of the *S. cerevisiae HIS3* promoter, was cut with BamHI and SpeI restriction enzymes to linearize the

plasmid. The *CLN3 scr2* amplified coding sequence was cloned into the cut AGB392 vector using NEBuilder HiFi DNA Assembly (New England Biolabs). Cloning was confirmed via sequencing (Genewiz) using 5' TGGTTATGGCGCCCTCACAG 3' and 5' GCCCATTAACATCACCATCTAATTC 3'. This plasmid was transformed into WT *A. gossypii* (AG416) via electroporation and selection on AFM+G418 plates.

Cell culture and Imaging

Ashbya cells were grown in 10 mL Ashbya full media (AFM) under selection of either G418 (200 ug/ml) or Clonat (100 ug/ml) in a 125 ml baffled flask shaking at 30°C for 16 hours. The cultures were then transferred to 15 ml conical tubes (VWR) for centrifugation at 350 rpm for 2 min. AFM was removed and cells were suspended in 10 ml 2X Low Fluorescence media. Cells were then placed on a 2X Low Fluorescence media gel-pad containing 1% agarose embedded in a depression slides, sealed with valap and imaged. For dye incorporation experiments, *Ashbya* cells encoding a Whi3 HaloTag were spun down, washed with 2X Low Fluorescence Media and then incubated with 62.5 nM JF649 Halo dye (Lavis Lab, Janelia Farms Research Campus) for 20 min. The cells were then washed twice before being placed on gel pads and imaged at indicated time intervals. Image intensity for each droplet was quantified by finding the highest intensity pixel within the droplet and then taking the average intensity of a circle of about 9 pixels around the highest intensity pixel. All image processing and analysis for *in vivo* experiments was carried out in either Fiji or MATLAB (*19, 20*). For Whi3-tomato measurements, N=2 independent experiments with n=4 cells, 73 perinuclear droplets and 27 tip droplets were measured and for Whi3-Halo, N=2 independent experiments n=7 cells, 40 perinuclear droplets and 15 tip droplets were measured.

Single molecule RNA F.I.S.H and Imaging

RNA smFISH labeling was performed as previously described (*12*). Briefly, cells were grown overnight at 30 °C in AFM and were fixed using 3.7% (vol/vol) formaldehyde (Fisher Scientific) and then washed twice with cold buffer B. Cells were resuspended in 1mL of spheroplasting buffer and digested using 1.5 mg/ml Zymolyase (MP Biomedicals) for 30 min at 37 °C. Cells were washed twice with buffer B, and then treated with Proteinase K for 5 min to digest proteins and unmask protein-bound RNAs. Cells were then washed twice before being resuspended in 70% ethanol, and incubated overnight at 4 °C. Cells were washed twice with SSC wash buffer before being resuspended in hybridization buffer containing Tetraethyl rhodamine (TAMARA) or cy5-conjugated RNA FISH probes (Stellaris LGC Biosearch Technologies) complementary to each transcript of interest. Cells were incubated in the dark overnight at 37 °C. After incubation, cells were washed once with wash buffer, incubated with 5 ug/ml Hoechst (Invitrogen) and incubated at room temperature for 30 min before being washed a final time with wash buffer, mounted on glass slides with 20 ul Prolong Gold mounting medium (Invitrogen), sealed with nail polish, and then imaged. Images were de-convolved using 29 iterations of the Lucy-Richardson algorithm on Nikon Elements software and then processed in Fiji.

Analysis of mRNA fraction co-localized

A 8 X 10 ROI was generated at the tips of hyphae or around individual nuclei in merged images. Percent of co-localization was determined by counting the presence of overlapping signal from

each of the individual mRNA channels. A total of 40 tips and nuclei were used for analysis and taken across at least 2 biological replicates. mRNAs inside the nucleus were counted and co-localization events inside the nucleus were counted as well.

Recombinant Protein Expression and Purification

Protein purification was performed as previously described (*3*). In brief, full length Whi3 or whi3-Y610-F653A was tagged with an N-terminal 6-Histidine tag and expressed in BL21 *E. coli* (New England Biolabs). For labeled protein, full length Whi3 was tagged with a C-terminal GFP. Cells were lysed in lysis buffer (1.5M KCl, 20 mM Tris pH 8.0, 20 mM Imidazole pH 8, 1 mM DTT, 1 tablet of Roche protease inhibitor cocktail). The supernatant was incubated and passed over a Ni-NTA resin (Qiagen) in gravity columns. The resin was then washed with 10CV lysis buffer and protein was eluted with 6CV elution buffer (150 mM KCl, 20 mM Tris pH 8.0, 200 mM Imidazole pH 8.0,1 mM DTT). The fractions containing Whi3 protein were dialyzed into fresh droplet buffer (150 mM KCl, 20 mM Tris pH 8.0, 1 mM DTT) and measured with Bradford reagent. Aliquots of protein were flash frozen and stored at -80 ºC.

RNA Transcription

The T7 promoter 5' TAATACGACTCACTATAGGG 3' was cloned into the 5' end of *CLN3* (AGB 690), *BNI1* (AGB 691), and *SPA2* (AGB 692). The *cln3*-scr plasmid was synthesized with the T7 promoter (IDT). Plasmid DNA was digested with restriction enzymes to obtain a linear DNA template that was then transcribed using T7 Hiscribe *in vitro* transcription kit (NEB)

according to manufacturer's instructions. To obtain labeled RNA for imaging, 0.1 ul of 5 mM cy3-UTP or cy5-UTP (GE Healthcare) was added into the transcription reaction. Transcribed RNAs were then treated with DNase, precipitated with LiCl, and washed with 85% ethanol before being re-suspended in TE buffer and stored at -80 ℃.

Droplet Assembly and Imaging

Whi3 used in experiments contain 10:1 unlabeled to GFP-labeled protein. For recruitment experiments, Whi3 protein and cy5 labeled *BNI1* RNA were mixed and incubated for four hours in glass chambers (Grace Bio-Labs) at room temperature to desired concentrations in droplet buffer. The chambers were pre-treated with 30 mg/mL BSA (Sigma) for 30 minutes. After four hours, cy3-labeled RNA of interest was added to the wells, mixed, and incubated for 30 min. Imaging of droplets was done either on a spinning disc confocal microscope (Nikon CSU-W1) with VC Plan Apo 60X/1.49 NA oil immersion objective and an sCMOS 85% QE camera (Photometrics) or a custom spinning disk confocal microscope (Nikon Ti-Eclipse equipped with a Yokogawa CSU-X spinning disk module) using a 60X 1.49 NA oil immersion objective and an air-cooled EM-CCD camera. For the RNA melting experiments, RNA was denatured at 95 ℃ for three minutes and then immediately added to preformed droplets. For the RNA refolding experiments, RNA was denatured at 95 ℃ for three minutes and then cooled down at 1-4 ℃ per minute to 37 ℃ final temperature in a thermocycler, added to preformed droplets, and imaged immediately. For the *BNI1* melted experiments, *BNI1* mRNA was heated to 95 ℃ for 3 minutes before being mixed with Whi3 and incubated for 2 hours. *CLN3* mRNA was then added and immediately imaged. For the *CLN3* oligonucleotide experiments, 5 nM *CLN3* was mixed with a

100 nM mixture of the 5 oligo nucleotides (Supplemental Table 2). This mixture was then melted to 95 °C for 5 min then cooled to 70 °C (average melting temperature for the 5 oligos) for 10 min in a thermocycler before being added to *BNI1* droplets and imaged. For the *SPA2* oligonucleotide experiments, 5 nM of *SPA2* was mixed with a 100 nM mixture of the 4 oligo nucleotides (Supplemental Table 2). This mixture was then incubated at 25 °C for 10 min in a thermocycler before being added to *BNI1* droplets and imaged. At least five independent imaging areas were analyzed for each condition for each replicate. Data shown are representative of three or more independent replicates, across at least two RNA and protein preparations.

RNA Spermine experiments and analysis

For RNA spermine experiments, 10 nM *in vitro* transcribed mRNAs were incubated for 4 hours in Spermine buffer (10 mM Spermine tetrahydrochlroide (Sigma), 20 mM KCl, 10 mM $MgCl_2$) as previously described (*14*) and then imaged on a custom spinning disk confocal microscope (Nikon Ti-Eclipse equipped with a Yokogawa CSU-X spinning disk module) using a 60X 1.49 NA oil immersion objective and an air-cooled EM-CCD camera. For the RNA melting experiments, both *BNI1* and *CLN3* were melted for 3 minutes at 95 °C before being mixed together and incubated for four hours. For the *CLN3* oligonucleotide experiments, 10 nM *CLN3* was mixed with a 100 nM mixture of the 5 oligo nucleotides. This mixture was then melted to 95 °C for 5 min then cooled to 70 °C for 10 min in a thermocycler before being added to wells to incubate for four hours. For the *SPA2* oligonucleotide experiments, 10 nM of *SPA2* was mixed with a 100 nM mixture of the 4

oligo nucleotides. This mixture was then incubated at 25 ºC for 10 min in a thermocycler before being added to wells to incubate for four hours. Images were cropped to the middle 11 z stacks. Cy3 and cy5 channels, representing the different RNAs, were split and each channel was background subtracted with a 100-pixel rolling ball. Data shown are representative of three or more independent replicates, across at least two RNA preparations. The ImageJ plugin "JACoP" (https://imagej.nih.gov/ij/plugins/track/jacop.html) was used to calculate the Pearson's Correlation Coefficient between the two background-subtracted channels. The Wilcoxon Rank Sum Test was used to test for statistical significance between experimental conditions.

The DNA oligonucleotide sequences (IDT) used are as follows.

CLN3 to *BNI1*:

30 mer 461-479:	5'tcaaagTGCGCATCTCCACGGTAAGttccg 3'
30 mer 748-758:	5'cagagcacaCAGACCAGTTAaggctcttga 3'
30 mer 969-992:	5'ctaTGAACTCGGAGAGCTCAGCGAGTCgga3'
30 mer 1225-1248:	5'gcaCTGTCCGGTGCtGAGCCTGCACATggc 3'

SPA2 to *BNI1*:

30 mer *55-85*:	5' GGGTCGAGCTTagacctgggcgcaggcatt 3'
30 mer 1266-1296:	5' gtcgaaAGTGATGATATCAACAGaggatgg 3'
30 mer 4173-4203:	5'tcgggcTGCTTCTCCAGGATCATtggtgtc 3'
30 mer 4294-4324:	5' tcgcctTTTAATTTTGAGACTTCatcaggg 3'
30 mer 10018-10048:	5' tcgaatataAGCCGCACCGCCtcccactct 3'

Analysis of RNA Recruitment

We calculated a Recruitment Coefficient (RC) for RNAs added into preformed Whi3-*BNI1* droplets which is defined by the following equation:

$$RC = \frac{[RNA]_{PD}}{[RNA]_O}$$

where RC is the recruitment coefficient, $[RNA]_{PD}$ is the concentration of added RNA (cy3) within the preformed droplets, $[RNA]_o$ is the concentration of added RNA (cy3) outside the preformed droplets. A higher RC indicates that the RNA is more concentrated in preformed droplets. All image analysis was performed using Fiji. To obtain the concentration of RNA, image channels were split into preformed droplets (cy5) and added RNA (cy3). A mask was created on the preformed droplet channel after background subtraction. Droplets were identified using the 3D objects Counter plugin, with intensity threshold of 1480 for data acquired on the Yokogawa CSU-X and 100 for data acquired on the Nikon CSU-W1. This method was used to obtain the integrated density of the cy3 channel and the area of the preformed droplets. Average mean fluorescent intensity (MFI) of preformed droplets was then calculated as the sum of integrated density across the z-stack volume divided by sum of area across the z-stack volume. Then, per z-stack volume, inverse selection of preformed droplets is measured for integrated density and area. Average MFI outside preformed droplets calculated as above. MFI values are converted to dye concentration using linear fit of a concentration curve of cy3 dye (one for each instrument). RNA concentrations were obtained by normalizing the dye concentration by the average number of dye molecules incorporated into each different RNA. To calculate significance between different RNAs, unpaired t tests were performed on log-transformed RC values between experimental conditions in R version 3.4 (*21*).

Analysis of Whi3 to RNA ratios

Whi3-RNA droplets were imaged, as previously described, over the course of four hours, starting thirty minutes after the addition of the RNA to Whi3. Image analysis was performed in Fiji. For each time point, the RNA and Whi3 channels were split, background subtracted, and 3D object counter was used to measure the MFI of both RNA and Whi3 channels separately. MFI values for RNA and Whi3 were then converted to concentrations based on a linear GFP or RNA dye curve. Whi3 concentrations were corrected for the unlabeled protein present. For each time point, the average concentration was calculated and then the ratio of Whi3 to RNA was calculated as the average Whi3 concentration divided by the average RNA concentration. The standard deviation of the ratio was calculated based on the following equation:

$$SD = \sqrt{\frac{Var(Whi3)}{Whi3^2} - 2 \times \frac{Whi3}{RNA^3} \times Cov(Whi3,RNA) + \frac{Whi3^2}{RNA^4} \times Var(RNA)}$$

where Whi3 is the concentration of Whi3, RNA is the concentration of RNA, Var(x) is the variance of variable x, and Cov (x, y) is the covariance of variables x and y.

SHAPE-MaP experiments and Analysis

SHAPE-MaP was performed as previously described (*15*). In brief, 500 ng of *in vitro* transcribed RNA was added to one-ninth volume of 1M7 or neat DMSO (10 mM final concentration) and

incubated at room temperature for 10 minutes. RNAs were exchanged into TE buffer (10 mM Tris-HCl, 1 mM EDTA) (Ambion) using a desalting column (GE Life Sciences). For *CLN3*, *CLN3* refolded, *cln3 scr*, *cln3 sm*, *BNI1* and *SPA2* mRNAs, modified (1M7) and untreated (DMSO) RNAs were subjected to mutational profiling (MaP) reverse transcription with a random primer (200 ng/ ul R9, NEB). The resulting cDNA was purified (Agencourt RNACLean XP beads, Beckman Coulter) and prepared for library construction by second strand synthesis module (NEB). These cDNAs were then used in amplicon library preparation using Nextera XT indices 1 and 2 and tagmentation and PCR protocol. *CLN3* that was modified with 1M7 or incubated with DMSO in the presence of Whi3 protein (2 uM Whi3, 27 nM *CLN3*), was heated to 95 °C to denature the proteins and RNA was recovered and purified with RNAClean XP beads. The RNAs were subjected to mutational profiling (MaP) reverse transcription with a gene specific primer (5' CGGCTGGGACTGGAAGC 3'; IDT) to amplify the first 500 nucleotides of the mRNA. Sequencing libraries were created with CLN3 and Whi3 + CLN3 amplicons using IDT gene specific primers F1 (5' GACTGGAGTTCAGACGTGTGCTCTTCCGATCT NNNNNGTCTGCATACCAAGGATCAGC 3') and R1 (5' CCCTACACGACGCTCTTCCGATCTNNNNNCGGCTGGGACTGGAAGC 3'). Libraries were purified using DNA beads (Agencourt) and sequencing libraries were pooled and then sequenced on an Illumina MiSeq instrument. SHAPE reactivity profiles were created by aligning the RNA reference sequence using ShapeMapper v 0.15 (www.chem.unc.edu/rna/software.html). Default parameters were used and the folding module was not used. RNA structural modeling was created by Superfold with 1M7 reactivities under default parameters and deltaSHAPE was calculated and plotted using deltaSHAPE software (www.chem.unc.edu/rna/software.html).

RNA secondary structure arc plots were drawn with recently developed tools implemented in the Integrative Genomics Viewer (*22*).

Median read depths are reported in **Table S1**.

RNA	Modified read depth	Untreated read depth
CLN3	88,775	31,645
CLN3 refold	15,989	15,380
cln3 scr	38,418	32,906
cln3 sm	101,590	98,472
BNI1	27,147	38,362
SPA2	20,936	9,314
CLN3 (amplicon)	233,978	219,741
CLN3 + WHI3 (amplicon)	37, 236	128,531

Table S1. Median read depth for modified and untreated SHAPE-MaP experiments.

Single Molecule FRET experiments and Analysis.

A custom-built total internal reflection fluorescence (TIRF) microscope was used for all single molecule fluorescence assays. Lasers of different wavelengths were used to excite different fluorescent dyes. For FRET experiments involving Cy3 (donor) and Cy5 (acceptor) dyes, a solid state 532nm laser (75mW, Coherent CUBE) was used to excite the donor dye. For the counting of GFP photobleaching steps, a 488nm laser (50mW, Coherent Sapphire) was used. For FRET imaging, the emitted signals were separated by dichroic mirrors with a wavelength cutoff of 630nm to separate the Cy3 and Cy5 emissions. The signals were then detected by an EMCCD camera (iXon DU-897ECS0-#BV; Andor Technology). The camera was controlled via a custom C++ program, and single molecule traces extracted recorded data using IDL software. Single molecule traces were then displayed and analyzed using Matlab and Origin software. All code can be found in the single molecule FRET (smFRET) package available at the Center for the Physics of Living

Cells (https://cplc.illinois.edu/software/, Biophysics Department, University of Illinois at Urbana-Champaign).

RNA substrate prep

Single strand RNAs were ordered from Integrated DNA Technologies (Coralville, IA, USA) containing amino modifier at the labeling site. The RNAs were labeled using Cy3/Cy5 monofunctional NHS esters (GE Healthcare, Princeton, NJ, USA). Then, 10 nmol of amino modified oligonucleotides in 50 ml of ddH$_2$O and 100 nmol of Cy3/Cy5 NHS ester dissolved in DMSO was added and incubated with rotation overnight at room temperature in the dark. The labeled oligonucleotides were purified by ethanol precipitation.

For FRET experiments, *CLN3* and *BNI1* FRET RNA partial duplex RNA substrates were composed of dsRNA consisting of 18 bps of random CG-rich sequences and ssRNA consisting of truncated versions of *CLN3* or *BNI1* RNA. A Cy5-Cy3 FRET pair was placed at the junction and the 3' end of the ssRNA, respectively (Fig. 4C).

The RNA sequences used are as follows.

18mer for *CLN3*: 5' – Biotin – UGG CGA CGG CAG CGA GGC – Cy5 – 3'

CLN3 RNA: 5' – Cy3 – UAC CUG CAC GCG GUC GAG ACG UCU GCA UAC CAA GGA
          UCA GCC GCU UGC AUU AAA GGG GAC GAA CCG GGG C GCC UCG CUG
          CCG UCG CCA – 3'

18mer for *BNI1*: 5' – Biotin – ACC GCU GCC GUC GCU CCG – Cy5 – 3'

RNA: 5' – Cy3 – AUA UUC UAC AUG AUU AUG AUG CAU UAG AGA AGG AAA ACG

CCU ACU AUA AGU GUU UGA GAG UCC AUA UUC UAC AUG AU CGG AGC

GAC GGC AGC GGU – 3'

RNA substrates were annealed by mixing the biotinylated and non-biotinylated oligonucleotides in a 1:2 molar ratio in T50 buffer (50mM NaCl, 10mM Tris-HCl (pH 8.0)). The final concentration of the mixture was 10uM. The mixture was then incubated at 95°C for 2 minutes followed by slow cooling to room temperature to complete the annealing reaction in just under two hours. The annealed RNAs were diluted to 10nM single molecule stock concentration and stored at -20°C.

All experiments were performed in Whi3 Reaction Buffer (150mM KCl, 50mM Tris-HCl (pH 8.0), 1mM DTT) with an oxygen scavenging system containing 0.8% v/v dextrose, 1 mg/ml glucose oxidase, 0.03 mg/ml catalase[1], and 10mM Trolox. All chemicals were purchased from Sigma Aldrich (St. Louis, MO). The experiments were all performed at room temperature. Fifty to 100pM of biotinylated FRET RNA were immobilized on polyethylene glycol (PEG)-coated quartz surface via biotin-neutravidin linkage.

Whi3-RNA FRET experiment

Whi3 proteins were prepared as described above. Then, 0.5 to 5uM of Whi3 or whi3-Y610-F653A proteins in droplet buffer was added to immobilized RNA substrates, and 10-20 short movies (10 seconds) and 3-4 long movies (2 minutes) were then taken to monitor the Cy3 and Cy5 emission

intensities over time. These are then analyzed to produce the FRET histograms and trajectories shown in Fig. 4D.

Dip-to-dip FRET fluctuation dwell times were collected between each successive dip in the FRET trace. These time intervals were then fitted to a single exponential decay function using Origin (OriginLab Corporation, Northampton, MA) to extract the half-life for each protein-RNA combination.